Effect of Molecular Guest Binding on the d-d Transitions of Ni(2+) of CPO-27-Ni: A Combined UV-Vis, Resonant-Valence-to-Core X-ray Emission Spectroscopy, and Theoretical Study

UNIVERSITÀ DEGLI STUDI DI TORINO

The Effect of Molecular Guest Binding on the *d-d* Transitions of Ni^{2+} of CPO-27-Ni: a Combined UV-Vis, Resonant Valence to Core XES and Theoretical Study

Erik Gallo,[1,2] Evgeny Gorelov,[3] Alexander A. Guda,[4] Aram L. Bugaev,[1,4] Francesca Bonino,[1] Elisa Borfecchia,[1] Gabriele Ricchiardi,[1] Diego Gianolio,[5] Sachin Chavan,[6] and Carlo Lamberti[4,7,*]

[1] Department of Chemistry, NIS and INSTM Reference Center, University of Turin, Via Quarello 15, I-10135 Torino, Italy.
[2] European Synchrotron Radiation Facility (ESRF), 6 Rue Jules Horowitz, BP 220 38043, Grenoble Cedex 9, France.
[3] European XFEL GmbH Holzkoppel 4, 22869 Schenefeld, Germany.
[4] International research Center "Smart Materials", Southern Federal University, Zorge Street 5, 344090 Rostov-on-Don, Russia
[5] Diamond Light Source Ltd, Harwell Science and Innovation Campus, OX11 0DE, Didcot, United Kingdom
[6] Department of Chemistry, University of Oslo, P.O. Box 1033 Blindern, N-0315, Oslo, Norway
[7] Department of Chemistry, CrisDi and INSTM Reference Center, University of Turin, Via P. Giuria 7, I-10125 Torino, Italy.

e-mail: carlo.lamberti@unito.it

ABSTRACT

We used Ni K-edge resonant valence to core X-ray emission spectroscopy (RVtC-XES, also referred to as direct RIXS), an element-selective bulk-sensitive synchrotron-based technique, to investigate the electronic structure of CPO-27-Ni metal-organic framework (MOF) upon molecular adsorption of significant molecular probes: H_2O, CO, H_2S and NO. We compare RVTC-XES with UV-Vis spectroscopy, and we show that the element-selectivity of RVtC-XES is of strategic significance to observe the full set of *d-d* excitations in Ni^{2+} which are partially overshadowed by the low-energy π-π^* transitions of the Ni-ligands in standard diffuse reflectance UV-Vis experiments. Our combined RVtC-XES/UV-Vis approach provides access to the whole set of *d-d* excitations allowing us a complete discussion of the changes undergone by the electronic configuration of the Ni^{2+}-sites hosted within the MOF upon molecular adsorption. The experimental data have been interpreted by multiplet ligand-field theory calculations based on Wannier orbitals. This study represents a step further in understanding the ability of the CPO-27-Ni MOFs in molecular sorption and separation applications.

1. INTRODUCTION

The ability to tune framework porosity, topology as well as framework compositions have made zeolites and zeotypes the most successful materials for a broad range of applications like gas adsorption/separation and catalysis. However, in the last few years, the role of zeolites as the leading class of crystalline porous materials has been challenged by a new emerging family: Metal Organic Frameworks (MOFs).[1]

Although the industrial application of MOFs is still limited to few cases,[2] this new class of materials is predicted to play an important role in the next future, in the fields of gas storage,[1d, 3] gas separation and purification,[4] gas sensors,[5] drug delivery,[6] optical materials,[7] magnetic materials,[8] solid state proton and ion conductors,[9] catalysis,[10] and materials for interim radioactive waste scavenging.[11]

In this work, we combined UV-Vis and hard X-ray resonant valence to core X-ray emission spectroscopy (RVtC-XES)[12] spectroscopies to shed light on the changes in the electronic structure of *d* orbitals of Ni^{2+} center in CPO-27-Ni upon molecular adsorption. Experimental results are supported with the non-resonant inelastic X-ray scattering (NIXS) and RVTC-XES spectra's calculation using multiplet ligand-field theory based on Wannier orbitals. This study represents a step further in the direction of understanding the adsorption phenomena that are behind the ability of the CPO-27-Ni (also known as MOF-74) class of MOFs in molecular sorption and separation applications.

1.1. CPO-27 MOFs for molecular sorption and separation

Gas sorption, separation and purification and catalytic applications require the availability of coordinatively unsaturated metal centers. CPO-27-Ni ($Ni_2(dhtp)(H_2O)_2 \cdot 8H_2O$, dhtp = 2,5-dihydroxyterephthalic acid, also known as MOF-74), fulfills this request.[13] CPO-27-M is a three-dimension honeycomb like framework with one-dimensional channels of about 11 Å diameter running along the *c* axis (see Figure 1). At the intersections of the honeycomb are helical chains of cis-edge connected metal oxygen octahedra running along the [001] direction. The first coordination shell of M^{2+} sites consists of five framework oxygen atoms while the sixth coordinative bond faces the channel and is available to coordinate ligand molecules, such as a water as shown in the inset in Figure 1. Several isostructural analogue of the framework with Mg^{2+}, Mn^{2+}, Fe^{2+}, Co^{2+}, Cu^{2+} and Zn^{2+} as a metal component have been reported.[13-14 15]

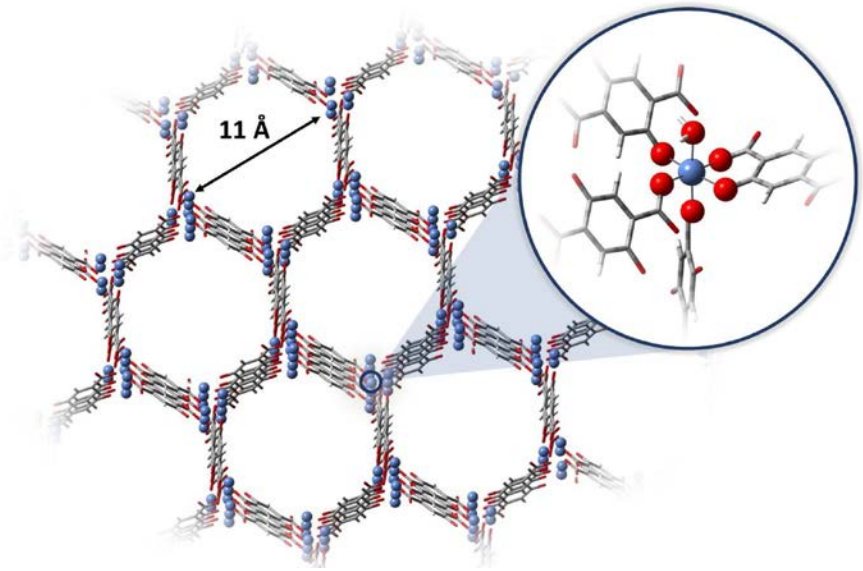

Figure 1. 3D representation of a dehydrated CPO-27-Ni structure, highlighting the honeycomb structure along the 1D channels of about 11 Å in diameter running along the [001] direction. The C atoms are reported in grey, H atoms in white, O in red, and Ni in blue. The inset reports a magnification of the first coordination spheres around a Ni^{2+} center (blue sphere) showing the five framework oxygen atoms (red spheres) and the coordination vacancy inside the channel saturated by a water molecule.

Upon solvent removal, CPO-27-M has a coordination vacancy at M^{2+} centers,[16] where guest molecules can be coordinated.[3a, 16-17] Molecular adsorption on CPO-27-M MOF has been widely investigated owing to the coordination vacancy at the metal site M. Among all, CO adsorption has been widely studied on CPO-27-Ni[15c, 17a, 17b] and on the equivalent Mg, Mn, Fe and Zn frameworks.[15c, 18] Authors found that the isostructural frameworks display isosteric heats of CO adsorption ranging from −52.7 to −27.2 kJ mol^{-1} (see Table 1) along the series Ni > Co > Fe > Mg > Mn > Zn, following the Irving−Williams stability order.[15c] NO adsorption was performed on CPO-27-Ni[16] and on CPO-27-Fe.[19] N_2 adsorption was investigated by Chavan et al. [17b] on CPO-27-Ni, and by Bloch et al.[20] on CPO-27-Fe; in the same work also O_2 adsorption was studied. H_2 adsorption was systematically studied at low temperature on isostructural MOFs CPO-27-M (M = Mg, Mn, Co, Ni, Zn).[3b, 21] Adsorption of CO_2 was investigated on the whole series of CPO-27-M.[3a, 15a, 22] Co-adsorption of H_2O and CO_2 was investigated by Mangano et al. on both CPO-27-Ni and -Mg.[23] CH_4 adsorption was studied by Dietzel et al. on Ni and Mg forms of CPO-27,[22a] while Chavan et al. investigated the adsorption of C_2H_4 on CPO-27-Ni[17b] and of C_2H_2 on the Fe, Co and Ni homologue frameworks.[24] Adsorption of H_2S was studied by Allan et al.[25] and by Chavan et al.[17d] The potential of the almost whole family of CPO-27-M MOFs (M = Mg, Co, Ni, Cu, and Zn) in the adsorptive desulfurization of fuels has been evaluated by De Vos group.[26]

Most of the reported literature also provided accurate determination of the adsorption enthalpy ($-\Delta H_{ads}$) measured either directly with microcalorimetry,[27] or indirectly via isosteric method[27a] or via variable temperature IR spectroscopy, that also provides the entropy of the adsorption process.[21b, 28] Other works are theoretical studies that have computed the corresponding adsorption energies ($-\Delta E_{ads}$). From a comparison of the energetic data ($-\Delta H_{ads}$ or $-\Delta E_{ads}$) for different molecules on the same material (see Table 1), the potential of CPO-27-M MOFs in gas separation applications is evident. In the following few specific examples are reported. (i) Bloch et al. concluded that that the CPO-27-M frameworks are promising materials for the separation of CO from various industrial gas mixtures, including CO/H_2 and CO/N_2.[15c] (ii) The same group,[20] highlighted that CPO-27-Fe is able to selectively bind O_2 over N_2 via electron transfer interactions at temperatures as high as 226 K, that is substantially higher than the cryogenic temperatures currently used to separate O_2 from air on a large scale. (iii) Valenzano et al. suggested CPO-27-Mg as a suitable material for CO/CO_2 separation.[15a] (iv) Chavan et al. indicates CPO-27-Ni as an

interesting material for the CH_4/C_2H_2 separation, which is of interest in the production of pure acetylene.[24] (v) Britt et al. indicates CPO-27-Mg as the best MOF for CO_2/CH_4 separation. (vi) Ghose et al.[29] showed that, for CPO-27-Ni, the temperature-dependent adsorption capacity of Xe is substantially larger than that for Kr, indicating the selectivity of Xe over Kr. (vii) The finding that H_2O is able to displace NO indicates that CPO-27-Ni(Fe) materials are of potential interest for gradual NO release in biomedical applications.[16, 19, 30] (viii) Rojas et al,[30a] used CPO-27-Ni for the incorporation and release of the [Ru(*p*-cymene)Cl_2(pta)] anticancer drugs. (ix) The possible use of CPO-27-Ni in adsorption water desalination application was highlighted by Elsayed et al.,[31] reporting a yield of 4.3 m^3·of water per day and per ton of material. (x) Finally, on the catalysis side, Xiao et al.[32] highlighted that CPO-27-Fe, and its magnesium-diluted analogue (CPO-27-$Fe_{0.95}Mg_{0.05}$) are able to activate the C–H bonds of ethane and convert it into ethanol and acetaldehyde using nitrous oxide as the terminal oxidant.

Table 1. Summary of literature studies, both experimental ($-\Delta H_{ads}$) end theoretical ($-\Delta E_{ads}$), reporting energetic aspects of molecular adsorption of different probes (CO, NO, H_2O, H_2S, CO_2, N_2, H_2, CH_4 C_2H_2) on M^{2+} sites of activated CPO-27-M MOFs M (M = Mg, Mn, Fe, Co, Ni, Zn). MC = microcalorimetry; IHA = isosteric heat of adsorption; VT-IR = variable temperature Infra Red; DFT = density functional theory; DBT dibenzothiophene . Reviewed theoretical studies have used the following DFT codes: CRYSTAL09,[33] VASP 5.3[34] and vdW-DF2.[35]

Molecule	Metal	$-\Delta H_{ads}$ or $-\Delta E_{ads}$ (kJ mol^{-1})	Method	Ref.
Xe	Ni	22	DFT	29
Kr	Ni	10	DFT	29
H_2	Mg	12	VT-IR	21b
H_2	Mg	9.4	VT-IR	36
H_2	Mg	10.1	IHA	21a
H_2	Mn	11	VT-IR	21b
H_2	Mn	8.8	IHA	21a
H_2	Mn	8.8	IHA	18a
H_2	Fe	9.7	IHA	18a
H_2	Co	13	VT-IR	21b
H_2	Co	11.2	VT-IR	37
H_2	Co	10.7	IHA	21a
H_2	Co	10.8	IHA	18a
H_2	Ni	15	VT-IR	21b
H_2	Ni	13.0	VT-IR	3b
H_2	Ni	19.9	IHA	21a
H_2	Ni	11.9	IHA	18a
H_2	Zn	10	VT-IR	21b
H_2	Zn	8.5	IHA	21a
CH_4	Ni	22	IHA	22a
CH_4	Ni	21.4	IHA	38
C_2H_2	Ni	48	MC	24
N_2	Ni	17	VT-IR	17b
N_2	Ni	27.3	DFT, CRYSTAL09	17c
N_2	Mg	21	VT-IR	15a
N_2	Mg	25.2	DFT, CRYSTAL09	15a
N_2	Fe	35	IHA	20
CO_2	Mg	47	IHA	39
CO_2	Mg	47	VT-IR	15a
CO_2	Mg	38.9	DFT, CRYSTAL09	40.
CO_2	Mg	43.5	IHA	22c
CO_2	Mg	40.9	DFT, vdW-DF2	22c
CO_2	Mn	31.7	IHA	22c
CO_2	Mn	33.9	DFT, vdW-DF2	22c
CO_2	Fe	39	IHA	22b
CO_2	Fe	33.2	IHA	22c
CO_2	Fe	34.1	DFT, vdW-DF2	22c
CO_2	Co	37	IHA	39
CO_2	Co	33.6	IHA	22c
CO_2	Co	33.8	DFT, vdW-DF2	22c

CO_2	Ni	41	IHA	[39]
CO_2	Ni	38	IHA	[22a]
CO_2	Ni	38.6	IHA	[22c]
CO_2	Nu	37.3	DFT, vdW-DF2	[22c]
CO_2	Cu	24	IHA	[15b]
CO_2	Cu	22.1	IHA	[22c]
CO_2	Cu	27.1	DFT, vdW-DF2	[22c]
CO_2	Zn	30	IHA	[41]
CO_2	Zn	26.8	IHA	[22c]
CO_2	Zn	30.2	DFT, vdW-DF2	[22c]
CO	Ni	58	MC	[17a]
CO	Ni	46.2	DFT, CRYSTAL09	[40]
CO	Ni	53.7	DFT, VASP 5.3	This work
CO	Ni	52.7	IHA	[15c]
CO	Mg	35.4	IHA	[15c]
CO	Mg	29	VT-IR	[15a]
CO	Mg	30.0	DFT, CRYSTAL09	[15a]
CO	Mn	29.7	IHA	[15c]
CO	Fe	43.6	IHA	[15c]
CO	Zn	27.2	IHA	[15c]
NO	Ni	90	MC	[16]
NO	Ni	49.1	DFT, CRYSTAL09	[17c]
NO	Ni	59.4	DFT, VASP 5.3	This work
H_2O	Mg	69.9	DFT, vdW-DF2	[42]
H_2O	Ni	74.7	DFT, CRYSTAL09	[17c]
H_2O	Ni	81.5	DFT, VASP 5.3	This work
H_2O	Zn	46.3	DFT, vdW-DF2	[42]
H_2S	Ni	57	MC	[17d]
H_2S	Ni	47.9	DFT, CRYSTAL09	[17d]
H_2S	Ni	66.0	DFT, VASP 5.3	This work
thiophene	Mg	2.5	MC	[26]
thiophene	Mg	55.4	DFT vdW-DF2	[26]
thiophene	Co	7	MC	[26]
thiophene	Ni	60.5	DFT vdW-DF2	[26]
thiophene	Ni	21	MC	[26]
thiophene	Co	55.9	DFT vdW-DF2	[26]
thiophene	Zn	48.8	DFT vdW-DF2	[26]
DBT	Mg	129.9	DFT vdW-DF2	[26]
DBT	Ni	135.8	DFT vdW-DF2	[26]
O_2	Fe	41	IHA	[20]

Restricting the discussion on the CPO-27-Ni material and on the molecules used in this study, $-\Delta H_{ads}$ values have been measured at 303 K by microcalorimetry for NO (92 kJ mol^{-1}),[16] CO (58 kJ mol^{-1})[17b] and H_2S (57 kJ mol^{-1}).[17d] Moreover, Bonino et al. have shown that H_2O is able to displace NO from Ni^{2+} sites in CPO-27-Ni; on these basis they have estimated adsorption enthalpy for water around 100 kJ mol^{-1}.[16] Summarizing, experiments have shown that the $-\Delta H_{ads}$ scale is $H_2S \sim CO < NO < H_2O$, see Table 1. Adsorptions of H_2S and CO are consequently classified in the physisorption category, while adsorption of NO and H_2O are chemisorption phenomena.

On the computational ground, the periodic calculations, including dispersion corrections, performed with the CRYSTAL09 code[33] using the B3LYP-D* method well confirmed the experimental trend ($H_2S \sim CO < NO < H_2O$).[17a, 17c] The calculations reported here, performed with the VASP code,[34] give adsorption energies in qualitative agreement with both experimental and previous CRYSTAL09 calculations with the only exception of H_2S, which adsorption energy is overestimated (Table 1).

The relevance of the molecular sorption and separation capabilities of the CPO-27-M class of materials makes it worth the development of advanced spectroscopic and theoretical approaches to understand the changes of the metal electronic configuration upon molecular adsorption. In the

present study, we report an in-depth experimental and theoretical study on the *d-d* transitions of Ni^{2+} centers in CPO-27-Ni upon adsorption of H_2O, CO, H_2S and NO molecules.

1.2. Investigation of *d-d* excitations in transition metal ions by RVtC-XES and UV-Vis spectroscopies

In this work we present an hard X-ray RVtC-XES (also referred to as direct-RIXS)[12] study of Ni^{2+} hosted in CPO-27-Ni MOF by measuring the evolution of the *d-d* transitions induced by adsorption of H_2O, CO, H_2S and NO. The use of hard X-rays allowed in situ measurements, which are not easily performed in the soft X-ray regime.[43] The experimental findings obtained at the ID26, beamline of the ESRF, were supported by means of theoretical calculations in the framework of the ligand field multiplet theory.[12a, 44] We remark that UV-Vis spectroscopy can access the *d-d* transitions and thus the final state observed with RVTC-XES (Figure 2b) because of vibronic-coupling: the *d-d* transitions are dipole forbidden.

We observed variations of the *d-d* transitions upon molecular adsorption on the Ni sites when water is replaced with other probe molecules. The desorption of the coordinated water molecule during the solvent removal procedure, as well as the adsorption of other molecules like CO, NO or H_2S modifies the ligand field, influencing the valence band (*d* levels) of the metal.[45] For several decades UV-Vis spectroscopy has been, and still is, the most used technique to measure *d-d* excitations for transition metal ions.[46]

UV-Vis spectra of model compounds have often been used to validate functionals and basis sets used by theoretical chemistry to compute occupied and unoccupied density of states.[47] The other way around, validated theoretical approaches have been used to identify unknown chemical species responsible for a given experimental UV-Vis spectrum.[48]

In UV-Vis spectroscopy, the *d-d* transitions (Figure 2b) of most of the systems are usually observed in the 0.5-3 eV region, although in some cases they may occur at lower energy. At higher energies, the spectra are commonly dominated by charge transfer (CT) transitions, that apart from very rare exceptions[49] are much more intense. This implies that for systems characterized by high-energy *d-d* and low-energy CT transitions the former may be overshadowed by the latter, and thus escape detection by UV-Vis spectroscopy. This is the case of the well-known nickel oxide (NiO) system. The $^3A_{2g}$ ground state of d^8 Ni^{2+} cations in O_h–like geometry is characterized by filled orbitals of t_{2g} symmetry and half-filled orbitals of e_g symmetry resulting in three dominant *d-d* transitions: $^3A_{2g}(F) \rightarrow {}^3T_{2g}(F)$; $^3A_{2g}(F) \rightarrow {}^3T_{1g}(F)$; and $^3A_{2g}(F) \rightarrow {}^3T_{1g}(P)$. The experimental UV-Vis spectrum of NiO,[50] here reproduced in Figure 5a, shows two clear components at 1.08 eV (8,700 cm^{-1}) and 1.85 eV (14,900 cm^{-1}) while the third one has not been directly observed because it is covered by the CT transitions. Zecchina et al.,[50] expecting the third component, attributed the shoulder in the CT edge around 3.5 eV (28,000 cm^{-1}) to the $^3A_{2g}(F) \rightarrow {}^3T_{1g}(P)$ excitation, see Figure 2 of the quoted work. Their intuition was qualitatively right, but actually, the expected third component occurs at 3.0 eV (24,000 cm^{-1}), as determined two decades later by Ghiringhelli et al.[51] and by Huotari et al.[52] using and RVtC-XES.[12, 43, 53] This result has been successively confirmed by van Veenendaal et al.[54]

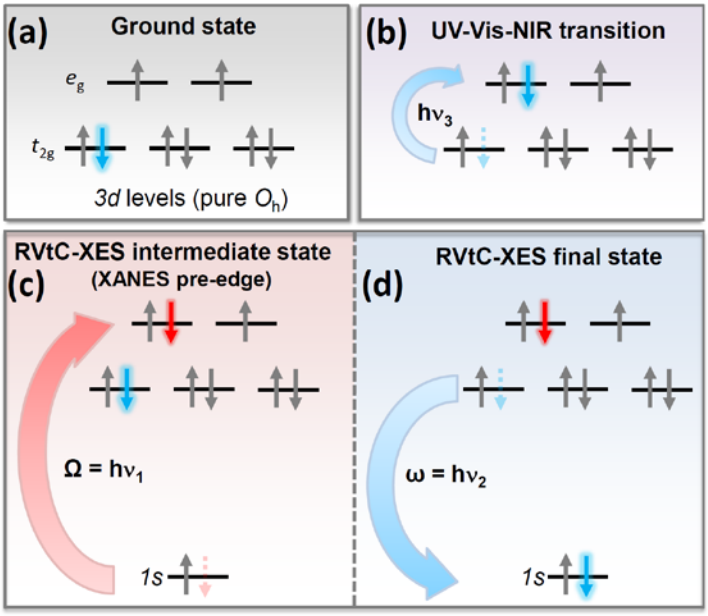

Figure 2. Simplified one electron schemes for Ni^{2+} ion (d^8) in O_h symmetry. Part (a): ground state. Part (b): final state after UV-Vis excitation (one-photon process). Part (c): final state after XANES excitation (one-photon process) and intermediate state of the RVtC-XES. Part (d): final state of the RVtC-XES excitation/deexcitation (two-photons process). Formally, the final states of (d) and (b) coincide, so that the simultaneous measure of Ω and ω probes the *d-d* transitions: $\Omega - \omega = h\nu_3$. Despite its simplicity for discussing the differences among the techniques, we remark that the one electron-scheme reported here cannot be used for discussing the experimental features observed in UV-Vis and RVtC-XES.

RVtC-XES, as all X-ray spectroscopies, is element-selective, and provides a means to probe the electronic states of materials[12, 43-44, 53, 55] in general and of transition metal-based catalysts in particular.[55g, 56] In order to clarify the comparison between UV-Vis and RVtC-XES we propose the simple one electron-scheme shown in Figure 2. In the ground state of Ni^{2+} in a perfect O_h-symmetry the t_{2g} levels are filled while e_g-levels have vacancies (Figure 2a).

On the experimental ground, RVtC-XES employs a primary monochromator (M in Figure 3) for selecting an exciting photon of energy $h\nu_1 = \Omega$ able to excite a core electron to an unoccupied level (Figure 2c). A core hole in the 1*s* orbital is therefore created and subsequently filled by an electron coming from some of the occupied states within the given lifetime. The transition can be radiative with emission of a photon of energy $h\nu_2 = \omega$ (given by the difference in energy between the two levels, Figure 2d). This process is generally referred to as X-ray fluorescence.

In general, in a total fluorescence yield (TFY) XANES experiment, the fluorescence X-rays emitted by the sample are collected by a standard photodiode (PD in Figure 3) or a solid-state detector. Owing to the absence (PD) or limited intrinsic energy resolution of the solid-state detector (typically, few hundreds of eV), it is not possible to take advantage of the chemical sensitivity of the emitted X-rays.

In a XES experiment together with the primary monochromator (M, already used for the standard XANES experiments) an additional spectrometer (composed of one or more crystal analyzers, CA in Figure 3) is used after the sample, acting as second monochromator. Using the Bragg reflection of the crystal analyzers, the photons emitted by the sample are selected with a total (i.e. incident convoluted with emitted) energy resolution in the 0.2-1.5 eV range, depending on the incident beam monochromator M and the emission spectrometer. The emitted (or scattered) photons can be collected by an Avalanche Photodiode Diode detector (APD in Figure 3). When a XANES experiment is carried out using such setup the total counts are lower compared to conventional fluorescence detected XANES spectroscopy, but the energy resolution that this experimental set up can reach is much higher, allowing to discriminate the origin of the different X-ray emission transitions and resolve chemical shifts.[12b, 56b, 57]

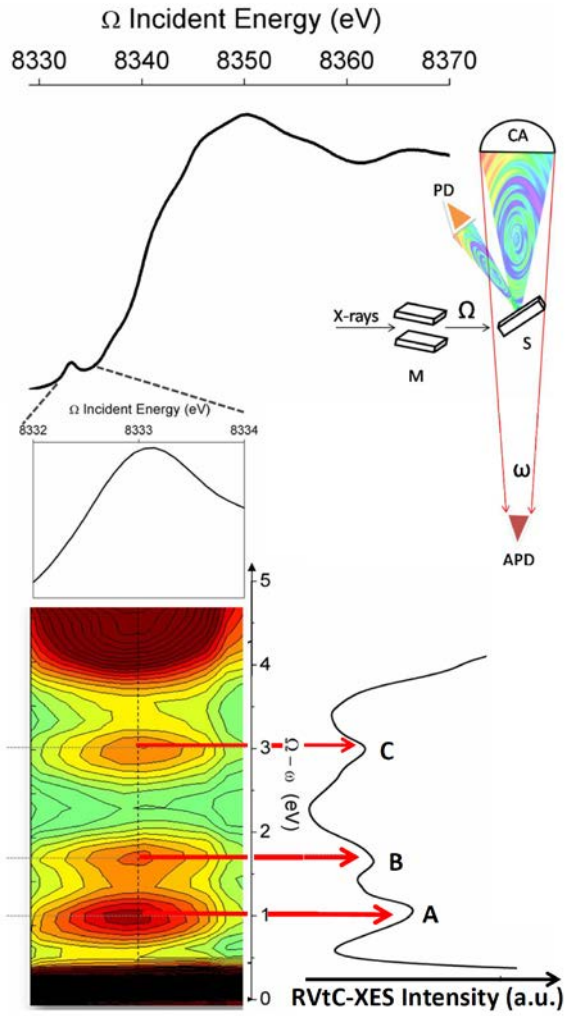

Figure 3. The scheme (top right) reports the standard set-up of a RVtC-XES experiment. The white X-ray beam emitted by the synchrotron is monochromatized by the primary monochromator (M), selecting the incident energy at $h\nu_1 = \Omega$ corresponding to an allowed transition at the Ni K-pre-edge. This photon yields a core hole in the 1*s* level of Ni (see Figure 2c). When a photodiode detector (PD) is adopted to collect the fluorescence of the sample, a scan of Ω across the Ni K-edge results in the standard XANES spectrum (top). If the fluorescence $h\nu_2 = \omega$, reaching the avalanche photodiode (APD) detector is discriminated with a crystal analyzer (CA), acting as second monochromator, then it is possible to distinguish among the different occupied states that contribute in filling the 1*s* core hole (Figure 2d). By scanning Ω over the pre-edge feature of the XANES spectrum (zoom in the mid left part) and ω over the Ω-ω region typical of *d-d* transitions, the RVtC-XES map (Ω/Ω-ω) can be obtained (bottom left corner for the NiO case). Finally, fixing the exciting energy Ω to the maximum of the XANES pre-edge peak, while scanning over ω, the atomic selective *d-d* transitions are obtained from the resonant X-ray emission (RVtC-XES, right bottom corner). Vertical red arrows indicates the maximum of the RVtC-XES spectrum i.e. the *d-d* transitions, labelled as **A**, **B** and **C**, bands according to the notation adopted by Huotari et al.[52]. (a.u. = arbitrary units).

When the incident X-ray energy Ω is tuned on the maximum of the pre-edge region of the K-edge XANES, the process can be referred to as RVtC-XES, or direct RIXS (bottom right corner in Figure 3). By spanning the whole pre-edge region, the collected spectra are Ω dependent, resulting all together into a RVtC-XES map (bottom left corner in Figure 3).

RVtC-XES spectroscopy has been used to investigate *d-d* transitions in several systems, mainly using the L[58] and K[52, 54, 55d, 59] metal edges, but in few cases also data from the M-edges have been reported.[58e, 60] Systems investigated by RVtC-XES concern: (i) oxides such as V_2O_3,[58f] TiO_2 and Li-doped TiO_2,[58b] MnO,[58d] Pd-modified TiO_2 nanotubes,[58i] CoO,[58e] NiO,[51-52, 54, 60b, 61] CuO_2,[59c] (ii) mixed oxides NaV_2O_5,[58a] La_2CuO_4,[59d] $LaMnO_3$,[58c, 59a] $La_{1-x}Ba_xMnO_3$ ($0.2 \leq x \leq 0.55$), $La_{0.76}Ba_{0.24}Mn_{0.84}Co_{0.16}O_3$, and $La_{0.76}Ba_{0.24}Mn_{0.78}Ni_{0.22}O_3$,[58c] $Zn_{1-x}Cu_xO$ (x = 0.03, 0.05, 0.07, and

0.10)[58g] CuB_2O_4,[59b] Na_2IrO_3 and Li_2IrO_3;[58h] (iii) halides NiF_2;[60b] (iv) mixed oxo-halides $Sr_2CuO_2Cl_2$;[59e, 60a] (v) covalent charged complexes $[Ni(II)(tfd)_2]^{=}$ and $[Ni(II)(tfd)_2]^{-}$ (tfd = $S_2C_2(CF_3)_2$);[60b] (vi) Ni-[55d, 59f] and Pt-containing[62] MOFs, and Cu-exchanged zeolites.[56n-r]

The pre-edge structure of transition metal ions is strongly dependent on the local symmetry of the ion.[43, 63] If a third-row ion has vacancies in the *d* states, like Ti(III, IV),[64] V(IV, V)[65] Cr(II, III, IV, VI),[48d, 66] Mn(II, II, IV, V, VII),[67] Fe(II, III),[55b, 68] Co(III, IV),[69] Ni(II, III)[16-17, 59f, 70] and Cu(II),[53, 71] then K-edge XANES spectra may show a weak 1*s*→3*d* pre-edge peak. The transition is usually very weak because it is dipole forbidden but quadrupole allowed. It becomes stronger when the ligand field implies a degree of 3*d*/4*p* hybridization.[43, 63c, 64a, 64e]

2. RESULTS AND DISCUSSION

2.1. Experiments

Figure 4a reports the 1*s*→3*d* pre-edge peak[72] of the XANES spectra of NiO (reference compound selected for this study) and of CPO-27-Ni with different guest molecules adsorbed on Ni^{2+} site. For samples with Ni^{2+} in an O_h-like geometry, the pre-edge (usually assigned to the 1*s*→3*d* transitions), lies around 8333.2 eV justifying the Ω value adopted to collect the RVtC-XES spectra (see vertical dashed line). The 5-fold coordinated Ni^{2+} of the dehydrated material (maximum at 8332.7 eV) shows a shift to lower energies and a broadening of the pre-edge feature indicating a splitting of the e_g orbitals. In the sample with NO bound to the metal center, the Ni^{2+} local environment is strongly modified owing to the high interaction energy (92 kJ mol^{-1}, see Table 1),[16, 17c] the 1*s*→3*d* transition shows a pronounced shift to higher energies. These shifts are linked to the different coordination (i.e. number and type of ligand) of the Ni^{2+} sites. Figure 4b reports the same spectra in the whole energy interval sampled on ID26 beamline, for verifying the absence of radiation damage of the samples. Due to this limitation, the standard normalization of the XANES spectra to the edge jump is not possible and we arbitrarily decided to normalize the spectra to the white line intensity. This procedure implies some distortion of the edge and post edge XANES features. For this reason we also report in Figure 4c the XANES spectra, collected in transmission mode on the BM29 EXAFS beamline (now moved to BM23) for the dehydrated CPO-27-Ni sample in vacuo and after interaction with H_2O, CO and NO.[16-17, 17c]

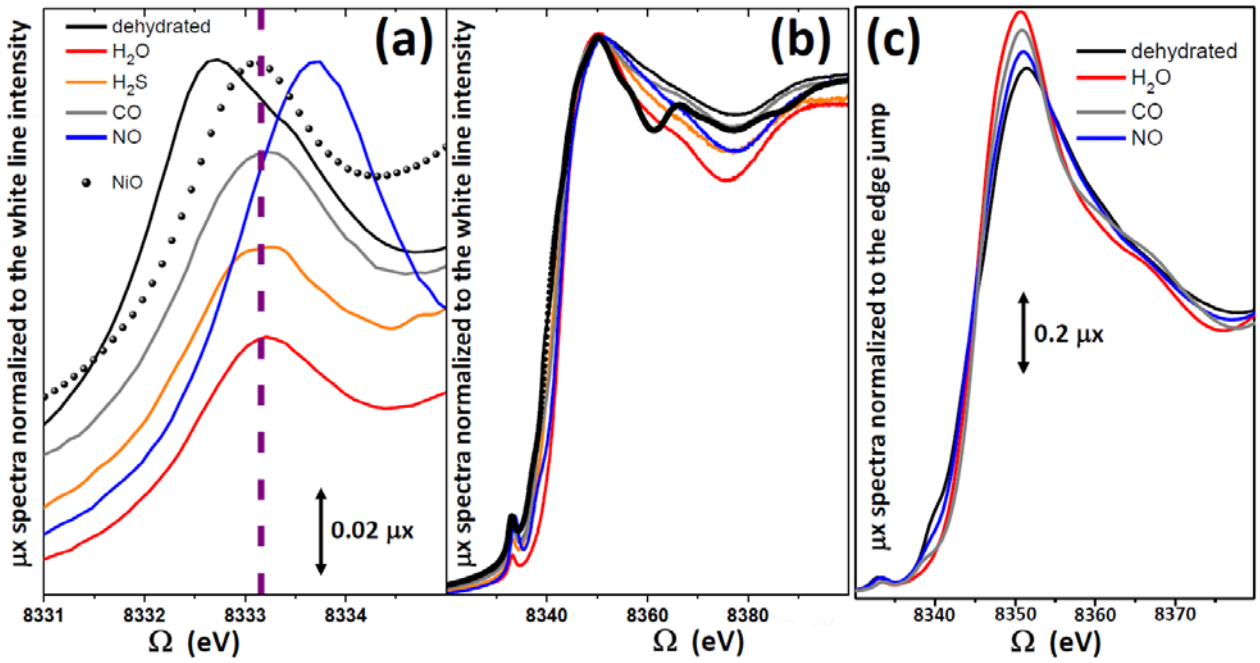

Figure 4. Part (a): Zoom on the 1*s*→3*d* pre-edge peak of the XANES spectra collected on ID26 in TFY mode of CPO-27-Ni MOF with different molecules adsorbed on the Ni^{2+} coordination vacancy: H_2O (red) H_2S (orange), CO (gray),

and NO (blue). The continuous black line refers to the activated material showing 5-fold coordinated Ni^{2+} species, while the black scattered dots refers to the spectrum of the NiO model compound. The vertical dashed line, centered on the maximum of the $1s \rightarrow 3d$ pre-edge peak of O_h-like Ni^{2+} species, shows the fixed Ω = 8333.2 eV energy value used to collect the RVtC-XES spectra reported in Figure 5. Spectra have been slightly vertically translated for clarity. Part (b): same TFY XANES spectra reported in part (a) plotted in the whole sampled energy scale. Part (c): standard XANES spectra collected in transmission mode on BM29 beamline of the ESRF. Same color code. Spectra in part (c) have been normalized to the edge jump, as usually done for XANES spectra.

The RVtC-XES spectrum of NiO (Figure 5a, blue curve), has been used as reference during our investigation. It shows three peaks labeled as **A**, **B** and **C** that can be interpreted using crystal field multiplet theory calculations, as already reported by Huotari et al.[52] The components **A**, **B** and **C** arise from $^3A_{2g}(F) \rightarrow {}^3T_{2g}(F)$; $^3A_{2g}(F) \rightarrow {}^3T_{1g}(F)$; and $^3A_{2g}(F) \rightarrow {}^3T_{1g}(P)$ transitions, respectively.[50, 52] We note that the **C** component is clearly visible in the RVtC-XES spectra, while it appears only as a shoulder in the CT edge of the UV-Vis-NIR spectra. Their energy position agrees with what was observed in previous RVtC-XES studies.[52, 54] The multiplet calculation performed by Huotari et al.,[52] foresaw a splitting of the bands that is large for **B**, smaller for **A** and almost negligible for **C** bands. The present work adopted an experimental setup with higher luminosity and lower energy resolution that is best suited for the study of dilute systems. The composite nature of component **B** is clearly evidenced by the asymmetry of the band observed in both RVtC-XES and UV-Vis-NIR spectra reported in the present work.

The RVtC-XES spectra of dehydrated CPO-27-Ni and of CPO-27-Ni upon adsorption of H_2O, CO, H_2S and NO are shown (blue curves) in Figure 5b-f. For direct comparison, the corresponding UV-Vis-NIR spectra (red curves) are superimposed. We used the **A**, **B** and **C** *d-d* excitations observed in the NiO model compound as reference to assign the features of the RVtC-XES spectra obtained for CPO-27-Ni with different molecules saturating the Ni^{2+} coordination vacancy.

From a direct comparison of the RVtC-XES spectra of NiO (Figure 5a) and CPO-27-Ni +H_2O (Figure 5b) we notice the presence of the same peaks revealing the O_h-like symmetry of the Ni^{2+} in the hydrated form of the MOF. In this case, the double nature of the **B** component results in two distinct maxima in the UV-VIS-NIR spectrum separated by 0.52 eV (Table 2). This value is larger than the one calculated by Huotari et al.,[52] for NiO (~0.2 eV). The sharp component at 0.644 eV (≈ 5200 cm^{-1}) and the shoulder at 0.868 eV (≈ 7000 cm^{-1}) observed in the UV-Vis-NIR spectrum are not due to electronic transitions but to the combination of ν and δ modes and to the first overtone of the ν mode of the water molecule, respectively.[73]

Table 2. Experimental Ni^{2+} *d-d* transitions in both RVtC-XES (XES) and UV-Vis-NIR (UV) spectra for NiO model compound, and for CPO-27-Ni with different guest molecules adsorbed on Ni^{2+} site, collected at Ω = 8333.2 eV. All reported values are in eV (1 eV = 8065.73 cm^{-1}). On the basis of the well-defined NiO model system, bands have been labeled as **A**, **B** and **C** according to the energy region where they were observed. To distinguish bands appearing in the same region, label prime has been added (**A'**, **B'**, **C'**). ObE = overshadowed by the elastic peak; ObCT = overshadowed by ligand to ligand charge transfer bands; "**–**" = not observed or not resolved; XES = RVtC-XES; UV = UV-Vis.

	A'	**A**	**B**	**B'**	**C**	**C'**
	XES/UV	XES/UV	XES/UV	XES/UV	XES/UV	XES/UV
NiO	–/–	1.1/1.07	1.7/1.81	–/–	3.0/~2.9	–/–
CPO-27-Ni + H_2O	–/–	1.0/1.16	1.8/1.68	–/1.89	3.1/~2.6	–/–
CPO-27-Ni + CO	ObE/0.61	1.1/1.11	1.7/1.64	–/–	3.2/~3.1	–/–
CPO-27-Ni + H_2S	–/–	1.1/1.17	1.8/1.89	–/–	3.1/ObCT	3.75/ObCT
CPO-27-Ni + NO[a]	ObE/0.61	1.1/1.11	1.9/1.80	2.5/ObCT	3.4/ObCT	–/–
dehydrated CPO-27-Ni[b]	ObE/0.71	1.2/1.27	–/1.76	–/–	3.1/ObCT	–/–

[a] RVtC-XES spectrum collected 0.5 eV out of the maximum (on the left side) of the $1s \rightarrow 3d$ pre-edge peak of the XANES spectrum (see blue curve in Figure 4a).

[b] RVtC-XES spectrum collected 0.7 eV out of the maximum (on the right side) of the $1s \rightarrow 3d$ pre-edge peak of the XANES spectrum (see black curve in Figure 4a).

The degassing process causes the loss of the H_2O molecule directly bonded to the metal center,[16] see inset in Figure 1, thus modifying the coordination of the Ni^{2+} from 6- to 5-fold. The peak **C** remains unaltered, while the peak **B** at 1.7 eV totally disappears in the RVtC-XES spectrum (see Section 2.2 for the theoretical explanation), being however clearly observed in the UV-Vis spectrum (Figure 5c). At the same time, new non-resolved transitions close to the elastic peak arise in the RVtC-XES spectrum. These transitions are well resolved in the UV-Vis-NIR spectrum resulting in peaks **A** and **A'**. These changes in the *d-d* excitations may be linked to the variation of the Ni^{2+} symmetry moving from O_h-like to C_{4v}-like symmetry, according to the ligand field theory.[16, 45, 74]

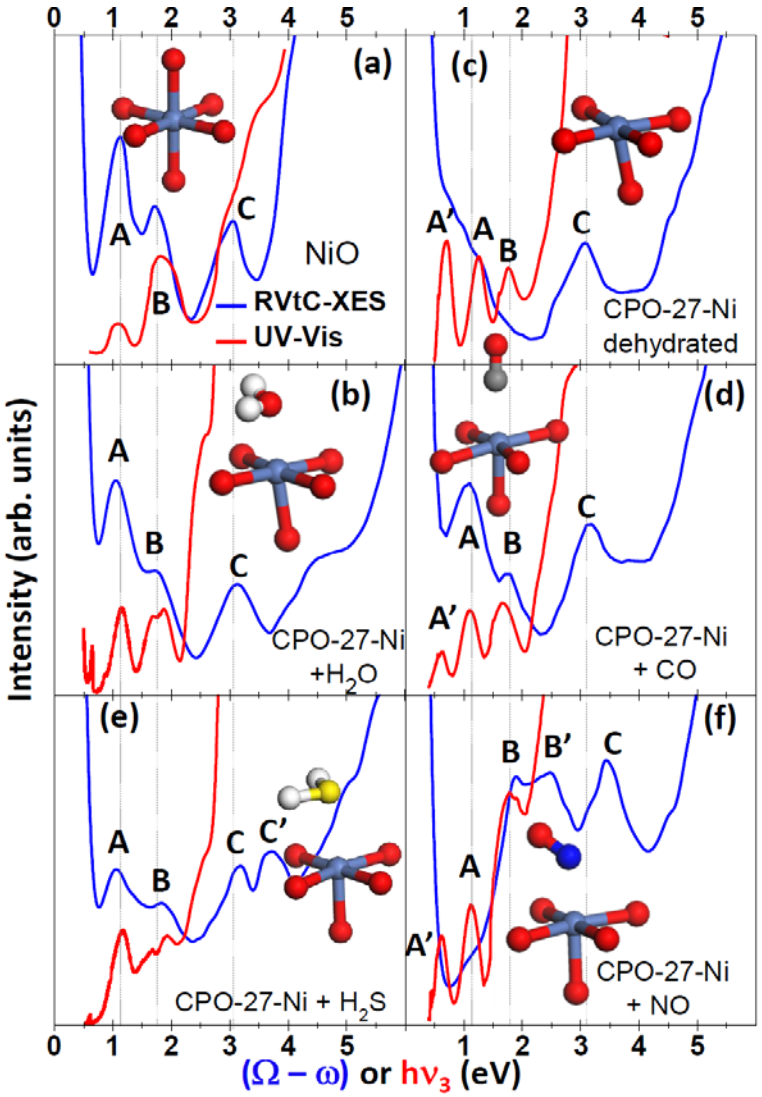

Figure 5. Direct comparison of UV-Vis-NIR (red curves, $h\nu_3$) and RVtC-XES (blue curves, Ω-ω) of (a): NiO model compound; (b) CPO-27-Ni + H_2O; (c): dehydrated CPO-27-Ni; (d): CPO-27-Ni + CO; (e): CPO-27-Ni + H_2S; (f): CPO-27-Ni + NO. Vertical dotted lines report the position of peaks **A**, **B** and **C** for NiO. For the exact positions of all labelled peaks see Table 2. The inset reports the first framework coordination shell and the adsorbed molecules as optimized in our periodic ab initio study. Color code as follows; Ni light blue; O red; N dark blue; C dark gray; S yellow; H white**.**

The RVtC-XES spectrum of CPO-27-Ni +CO (Figure 5d) is very similar to that observed in the CPO-27-Ni +H_2O case (Figure 5b), demonstrating that the O_h-like symmetry of the Ni^{2+} hosted in the framework is restored once CO is adsorbed. In the UV-Vis-NIR spectrum a lower energy peak (**A'** in Figure 5d) appears.

The same arguments adopted for CPO-27-Ni +H_2O could be used to describe the modification of the Ni^{2+} site upon adsorption of H_2S (Figure 5e). Also for CPO-27-Ni + H_2S the peak labeled **C** is overshadowed by the CT region in the UV-Vis-NIR measurement while is clearly visible in RVtC-XES. It is interesting to note that in this case we observe also an additional high energy peak (**C'**) between the *d-d*-transition and the CT region. According to the authors knowledge it is the first time that such peak is observed.

The strong interaction between the Ni^{2+} ions with the NO molecule introduces a further degree of complexity when treating the electronic structure of the system. In fact, the strong covalent chemical bond in the adduct profoundly modifies the ground state configuration of the *d*-levels above the Fermi energy of the CPO-27-Ni system. This is evidenced by a shift of the K pre-edge to higher energy and the utterly different *d-d* multiplet structure (Figure 4a and Figure 5f). A periodic study, performed with the CRYSTAL09 code at the B3LYP-D*/TZVP level of theory, of the interaction between NO and the Ni^{2+} of CPO-27-Ni has been recently performed.[17c] It has shown that, differently to CO, that adsorb in an end-on geometry, the angle between Ni-NO is bent (the angle optimized by DFT was 123°), resulting in an intermediate geometry between end-on and side-on. EXAFS study support the bent geometry of the adduct,[16, 75] that has been further confirmed by simulations of the XANES spectrum performed with the finite difference method.[76] The low Ni–N–O angle allows for maximizing the overlap between the NO molecular orbitals and the Ni e_g orbital.

The theoretical part reported in Section 2.2 will help us in the understanding of the *d-d* transition of CPO-27-Ni in presence of different adsorbates.

2.2. Computational modeling

Based on the adopted Hamiltonian, see Eq. (1) in Section 4.3, we calculated the non-resonant inelastic X-ray scattering (NIXS), that reveals the *d-d* excitations without the presence of the Ni(1*s*) core-hole, and the RVtC-XES spectra. In the RVtC-XES the initial state was Ni(1*s*), the intermediate states were Ni(3*d*) hybridized with ligands (framework oxygens and adsorbate) and the final state was Ni(1*s*). The transition operator used in calculation was $e^{i\mathbf{k}\cdot\mathbf{r}}$, thus including all multipole contributions, however dipole contribution is equal to zero in our model since *s-d* transitions are dipole forbidden and we didn't consider *p-d* hybridization. All computed spectra are reported, for the different cases, in Figure 6 as black and green curves for the RVtC-XES and NIXS calculations, respectively. Also reported, for direct comparison, are the experimental RVtC-XES spectra (blue curves).

Figure 6a refers to the NiO case, where Ni^{2+} are 6-coordinated in a perfect O_h symmetry. The NIXS theory (green spectrum) predicts the expected three bands at 1.05, 1.80 and 3.10 eV, corresponding to $^3A_{2g}(F) \rightarrow {}^3T_{2g}(F)$; $^3A_{2g}(F) \rightarrow {}^3T_{1g}(F)$; and $^3A_{2g}(F) \rightarrow {}^3T_{1g}(P)$ transitions respectively, already labeled as **A**, **B**, and **C** components in the discussion of the experimental spectra (Section 2.1). Due to different selection rules new features appear in the computed RVtC-XES (black spectrum), corresponding to transitions that are forbidden in the NIXS process. In particular, we observe a splitting of **B**s bands (at 1.65 and 1.81 eV) and a small feature appears at 2.67 eV between **B**s and **C**s components. This feature was already obtained in the atomic multiplet calculations of Huotari,[52] at 2.5 eV, without assignment. The limited energy resolution of the experimental spectrum (blue curve) does not allows us to reveal the five independents components predicted by the RVtC-XES theory (see Table 3), but the experimental broadening of **B** component is well compatible with the presence of **B** and **B'** peaks in the theory and low energy shoulder of peak **C** may be due to the weak component predicted in the theory at 2.67 eV

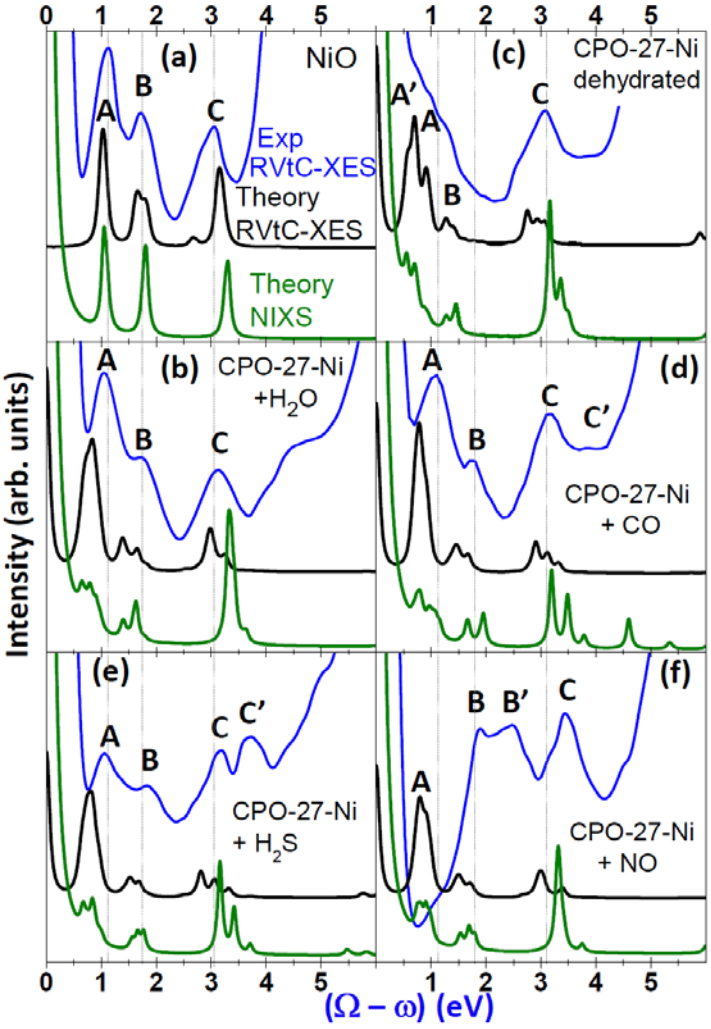

Figure 6. Direct comparison between experimental RVtC-XES (blue curves, same as in Figure 5) and theoretical (NIXS, green curves and RVtC-XES, black curves) spectra of: (a): NiO model compound; (b) CPO-27-Ni + H_2O; (c): dehydrated CPO-27-Ni; (d): CPO-27-Ni + CO; (e): CPO-27-Ni + H_2S; (f): CPO-27-Ni + NO. Labels **A'**, **A**, **B**, **B'**, **C** and **C'** refer to the experimental curves. Vertical dotted lines report the position of peaks **A**, **B** and **C** for NiO observed in the experimental spectrum. For the exact positions of the main peaks of the theoretical spectra see Table 3. Spectra have been vertically shifted for clarity.

Similar spectra are obtained in the case of CPO-27-Ni + H_2O, see Figure 6b. Since in this case we are dealing with a distorted O_h symmetry, theory predicts further splitting of the bands calculated for NiO. With respect to NiO, the shifts of **A** towards lower energies is qualitatively reproduced by theory, that however overestimate the value of the shift. Peak **B** appears at almost the same energy as in NiO, but loses intensity with respect to peak **A**; both evidences are well reproduced by the theory. Moreover, theory predicts a larger splitting between **B** and **B'** with respect to NiO (0.26 vs. 0.16 eV), a fact that may explain why this splitting has been observed in the UV-Vis-NIR spectrum, see red spectrum in Figure 5b. Finally, peak **C** undergoes a small blue shift with respect to NiO and theory predicts a splitting (not predicted in O_h symmetry), being the new **C** and **C'** peaks at lower and at higher energy with respect to the **C** peak in NiO. The presence of a CO or an H_2S molecule substituting H_2O in the first coordination shell of Ni^{2+} (Figure 6d or e) results in very similar **A**, **B** and **C** features on both experimental and theoretical sides, confirming a similar local structure around Ni centers. The main difference concerns the presence of high energy C' peaks; theory predicts an additional third peak in the C band, which is not present for adsorbed H_2O. The new C' peak clearly visible in case of H_2S, while it appears as an unresolved flat plateau in the case of CO. It must be however recognized that the theory underestimates the blue shift of this experimental new component. We must consequently consider our agreement on the high region side of these two spectra only qualitative. Our calculations for the CO and H_2S adsorbates

predicted larger splitting of the third peak C compared to the spectra of more octahedral systems (NiO or CPO-27-H_2O). However, the intensity of peak C in the experimental RVtC-XES spectra for H_2S and NO is larger than intensity of peak A (in contrast to opposite relation for NiO or CPO-27-H_2O) which we can explain by larger *p-d* hybridization on the Ni^{2+} metal center and corresponding *s-p* transitions that overshadow *s-d* transitions. Here only quardupole *s-d* transitions were taken into account.

Table 3. Main theoretical Ni^{2+} *d-d* transitions obtained with both RVtC-XES and NIXS calculations for NiO model compound, and CPO-27-Ni with different adsorbates. All reported values are in eV (1 eV = 8065.73 cm^{-1}). To allow a direct comparison with the experimental data (Table 2), bands have been labeled as **A**, **B**, **B'**, **C** and **C'** according to the energy region where they were observed. As calculations have no intrinsic energy resolution limitation, more bands can be assigned to the same label.

	A'	**A**	**B**	**B'**	**C**	**C'**
	RVtC-XES/NIXS	RVtC-XES/NIXS	RVtC-/NIXS	RVtC-/NIXS	RVtC-/NIXS	RVtC-/NIXS
NiO[a]	–/–	1.02/1.02	1.65/–	1.81/1.81	3.15/3.29	–/–
CPO-27-Ni + H_2O[a]	0.70/0.65	0.84/0.81	1.39/1.41	1.65/1.65	2.98/3.34	3.25/3.64
CPO-27-Ni + CO[a]	0.77/0.77	0.91/0.98	1.46/1.67	1.67/1.95	2.91/3.20	3.12/3.50 3.32/3.78
CPO-27-Ni + H_2S[a]	0.64/0.67	0.78/0.86	1.52/1.62	1.68/1.78	2.81/3.17	3.06/3.42 3.33/3.73
CPO-27-Ni + NO[a]	0.78/0.77	0.91/0.91	1.48/1.53	1.71/1.70	3.00/3.31	3.39/3.76
CPO-27-Ni + NO[b]		1.15/1.21	1.52/1.58	1.93/2.00 2.26/2.35	3.12/3.42	3.53/3.86 3.83/4.16
dehydrated CPO-27-Ni[a]	0.58/0.54	0.70/0.70 0.90/0.89	1.27/1.28	1.41/1.47	2.75/3.17	2.93/3.36 3.06/3.51

[a] Spectra calculation performed on a cluster extracted from the VASP optimized structure.

[a] Spectra calculation performed on a cluster extracted from the VASP optimized structure successively modified translating the NO molecule at a Ni-NO distance of 1.87 Å, as found by EXAFS.[16]

As already discussed in Section 2.1, removal of water causes great changes in the Ni^{2+} *d-d* transitions. In particular, experimental data reveal the new feature **A'** along with the apparent disappearance of peak **B**. Theory explains these facts as a shift of both peaks **A** and **B** to the lower energy along with additional splitting of the peak **A** with respect to NiO and hydrated CPO-27-Ni, see Figure 6c. In this way both **A**s and **B**s features contribute to the broad and unresolved experimental band below 2 eV. Experimentally, peak **C** exhibits an important shoulder at the low energy tail, that is well reproduced by the theory. Finally, our theory fails in describing the spectrum of adsorbed NO (Figure 6f). We attribute this failure to the fact that the adopted GGA-PBE exchange-correlation functional poorly reproduces the NO geometry in optimizations. Indeed, while for all other adsorbates the discrepancy between the experimental and computed adsorption distance is below 0.05 Å, in the case of NO, it is 0.24 Å, see Table 4 in Section 4.4. To partially overcame this problem both NIXS and RVtC-XES calculations have been repeated on a new structure obtained from the VASP output just translating the NO molecule in order to move the Ni–NO distance from 2.11 to 1.87 Å, that correspond to the value optimized in the EXAFS study of Bonino et al.,[16] and keeping the Ni–N–O angle equal to 123°. The results are reported as full black and full green curves in Figure 7, for the RVtC-XES and NIXS calculations, respectively. For comparison, Figure 7 reports also the experimental RVtC-XES spectrum (blue curve) and RVtC-XES and NIXS spectra computed on the VASP optimized structure (same as in Figure 6f).

Imposing a Ni–NO distance equal to 1.87 Å a significant improvement in the agreement between experiment and theory improves, in particular: (i) the position of the **A** component moves to higher energy and now matches the position of the experimental shoulder; (ii) in the 2-3 eV range, where the broad **B** and **B'** components appear in the experimental spectrum the previous RVtC-XES spectrum was totally flat, while in the black full line spectrum three components are present; (iii) the new RVtC-XES spectrum is also able to justify the region of the broad C component (3-4 eV range). Notwithstanding such a remarkable improvement in the prediction of the peak positions, the theory fails in predicting the correct relative intensity among the peaks, overestimating the intensity of **A** vs. **B**, **B'** and **C** peaks.

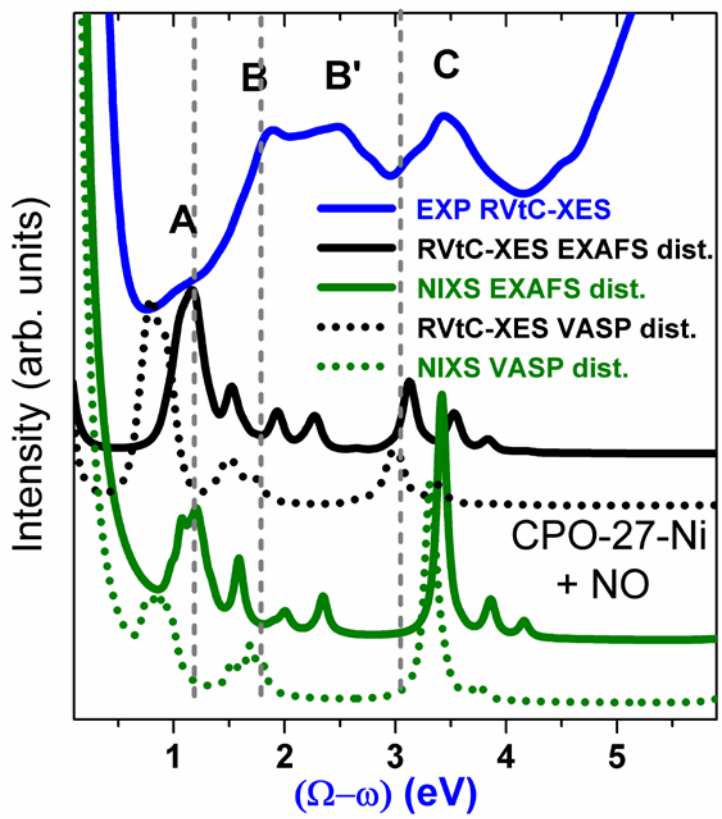

Figure 7. Direct comparison between experimental (blue curves, same as in Figure 5f) and theoretical (NIXS, green and RVtC-XES, black curves) spectra of CPO-27-Ni + NO computed using two different structures: VASP optimized structure (dotted curves, same as in Figure 6f) and structure extracted from the VASP optimized structure successively modified translating the NO molecule at a Ni-NO distance of 1.87 Å, as found by EXAFS[16] (full lines). Labels **A**, **B**, **B'** and **C** refer to the experimental curves. Vertical dotted lines report the position of peaks A, B and C for NiO observed in the experimental spectrum. For the exact positions of the main peaks of the theoretical spectra see Table 3. Spectra have been vertically shifted for clarity.

In a future work, we plan to perform a systematic optimization of the adsorption geometry, by looking to the best agreement between the experimental spectrum and theoretical one obtained by progressively changing both the Ni–NO distance and the Ni–N–O angle till convergence is obtained. Additional improvements may be also achieved including the Ni *p*-states in the spectral simulations, that are neglected in the present model that takes into account only *s-d* and *d-d* excitations, see Eq. (2) in Section 4.4.

3. CONCLUSIONS

Summarizing, the coupling of RVtC-XES and UV-Vis spectroscopies allows on one hand to investigate the entire *d-d* and charge transfer spectral region and on the other to discriminate the contributions of metal centers and linkers.[59f, 61, 77] This broad energy range is possible because there

are no limitations in the energy transfer range for resonant XES, while the flux of the standard UV lamps usually fades at 6-8 eV. A comparison between UV-Vis and RVtC-XES was performed in the 0.5-6.0 eV energy range, in order to observe the *d-d* excitations and the starting point of the charge transfer region. For all the investigated samples, the charge transfer transition appears at higher energy for RVtC-XES than for UV-Vis. The reason is that (besides *d-d* excitations) RVtC-XES only probes the ligand to metal plus the metal to ligand charge transfers while UV-Vis probes also the ligand to ligand excitations that arise at lower energy. The interpretation of the experimental RVtC-XES was supported by means of theoretical calculations within ligand field multiplet theory. Symmetry decrease from perfect O_h, results in band splitting predicted by theory and barely appreciated in experiment due to limited energy resolution. Theoretical spectra were able to reproduce well the experimental spectra (in terms of number of bands, energy position and their relative intensities) with the only exception of the case of NO adsorption. We believe that this failure is due to the inaccurate description of the Ni^{2+}-NO adduct from periodic DFT, that foresees an adsorption distance 0.24 Å larger than the experimental one (the error was below 0.05 Å on the other cases, see Table 4). Improvements in the agreement between experiment and theory were obtained by repeating the spectral calculation on a new structure where the Ni–NO distance was forced to be that optimized in the EXAFS refinement (1.87 Å).[16] On these basis, expect that, based on RVtC-XES spectra, structural parameters of adsorbates (adsorption geometries, distances and angles) may be optimized from iterative calculations on different geometries, similar to the procedure performed during XANES fitting.[56r, 76]

4. EXPERIMENTAL SECTION

4.1. Sample synthesis and structure control

The CPO-27-Ni material was prepared from a nickel(II) acetate and 2,5-dihydroxyterephthalic acid reaction in a THF–water solution to yield an ochre substance, $Ni_2(dhtp)(H_2O)_2 \cdot 8\ H_2O$, following the recipe reported in literature by Dietzel et al.[13b] XRPD patterns showed the high crystallinity of the sample and excluded the presence of undesired crystalline phases. A BET surface area of 1200 $m^2\ g^{-1}$ was measured by N_2 adsorption (Langmuir area 1315 $m^2\ g^{-1}$). The close coincidence between expected and measured surface area discards the presence of an undesired amorphous phases. Finally, Ni K-edge EXAFS confirms that, within the sensitivity of the technique, all Ni(II) has the expected local coordination environment in a sphere of 5 Å.[16-17] The concentration of Ni within the sample was of 23.6% in weight. CPO-27-Ni samples were pretreated under high vacuum at 393 K for 1 h.

4.2. UV-Vis, XES and XANES characterization

All the spectroscopic measurements were performed in controlled atmosphere by using *ad hoc* cells that allow thermal treatment in high vacuum, dosages and in situ spectra collection. CO, H_2S and NO gases were dosed at RT on the desolvated sample by means of an ad hoc conceived vacuum line. Before dosage, NO gas was carefully purified by distillation in order to remove other undesired nitrogen oxides. The solvated form of the MOF was used to probe the environment of Ni^{2+} in presence of coordinated water.

UV-Vis-NIR absorption spectra of NiO and of hydrated and activated CPO-27-Ni MOF were recorded in a reflectance mode by using an Agilent UV-Vis-NIR Cary 5000 spectrometer equipped with a diffuse reflectance attachment with integrating sphere of 15 cm in diameter coated by an highly reflecting florurated polymer. Prior to each measurement, baseline spectrum was collected by using Teflon as reference blank sample. Owing to the dispersive geometry of the instrument, the energy resolution is different in the different parts of the spectrum, moving from about 0.3 meV at 0.7 eV (where the first *d-d* transition is observed) up to 3 meV at 3 eV (where the first electronic transition of the linker occurs).

The X-ray emission experiments were performed at the high brilliance X-ray absorption and emission beamline ID26 of the European Synchrotron Radiation Facility (ESRF).[55c] The X-ray absorption experiments were performed using a Si(311) double crystal, cryogenically cooled, monochromator to select the excitation energy. High harmonics were suppressed using Si mirrors operating in total reflection. The RVtC-XES spectra were measured using the spectrometer available at ID26 based on Rowland geometry using five Si(551) crystal analyzers and an avalanche photodiode as detector. The distance between sample and analyzer crystals was 2 m, reaching a total resolution of 430 meV. The spot size on the sample was approximately 0.6 mm horizontally and 0.1 mm vertically. Because of the weakness of the investigated features, 20 RVtC-XES spectra were collected for each sample to increase the statistics, needing an overall acquisition time of 16 h for the averaged spectra reported in Figure 5b-f. Possible radiation damage of the samples has been carefully checked, as described in the following. On a short time-scale, XANES spectra have been collected on the same sample point both progressively decreasing the filter thickness absorbing the primary beam and increasing the integration time of a full XANES spectrum from 1 to 30 s. On a long time-scale, along the 16 h acquisition of the 20 RVtC-XES spectra we always collected a 30 s XANES spectra between two RVtC-XES spectra. We observed that CPO-27-Ni is stable under the photon power flux of ID26 independently of the dosed atmosphere (vacuum, H_2O, CO, NO, H_2S). Hence, no radiation protection macros (used to measure for a limited exposure time different points of the sample[56h, 78]) were adopted.

Standard XANES spectra (Figure 4b) were collected on the Ni K-edge at the BM29[79] beamline at the ESRF with a sampling step of 0.3 eV. The monochromator was equipped with two Si(111) flat crystals and harmonic rejection was achieved using Rh-coated mirrors after monochromator. The following experimental geometry was adopted: 1) I_0 (10% efficiency); 2) MOF sample; 3) I_1 (50% efficiency); 4) reference Ni foil; 5) I_2 (80% efficiency). This set-up allows a direct energy/angle calibration for each spectrum avoiding any problem related to little energy shifts due to small thermal instability of the monochromator crystals.[55g] Samples, in form of self-supported pellets of optimized thickness (corresponding to and edge jump at the Ni K-edge of $\Delta\mu x = 1.2$), have been located inside an ad hoc conceived cell developed at ESRF (by Prestipino, Steinman and Pasternack) that allows, evacuation, gas dosage and heating and cooling. On the chemical point of view, this experimental set-up guarantees the same degrees of freedom than that described in Ref.[80]

4.3. Structure optimization with the VASP code

Optimization of CPO-27-Ni geometry was performed with the VASP 5.3 code[34] using the PBE exchange-correlation potential.[81] The energy cutoff value of 400 eV was used for the plane-wave basis set. A 4x4x4 Monkhorst-pack grid for k-points was automatically generated resulting in 14 irreducible k-points. The choice of the k-points set was based on the energy difference between the calculation with 90 irreducible k-points and the calculations with lower number of irreducible k-points (see Figure 8). To consider the on-site Coulomb interactions for localized *d*-orbitals of Ni, the LSDA+U approach was applied.[82] The effective strength of Coulomb and exchange interactions, U and J, was set to 8.0 and 0.95 eV, respectively.[83] The dispersive interactions were considered using the DFT-D3 method of Grimme.[84] The convergence criterion for SCF calculations was set to 10^{-5} eV. The force smaller than 10^{-2} eV $Å^{-1}$ was used as a break condition for the ionic relaxation cycles.

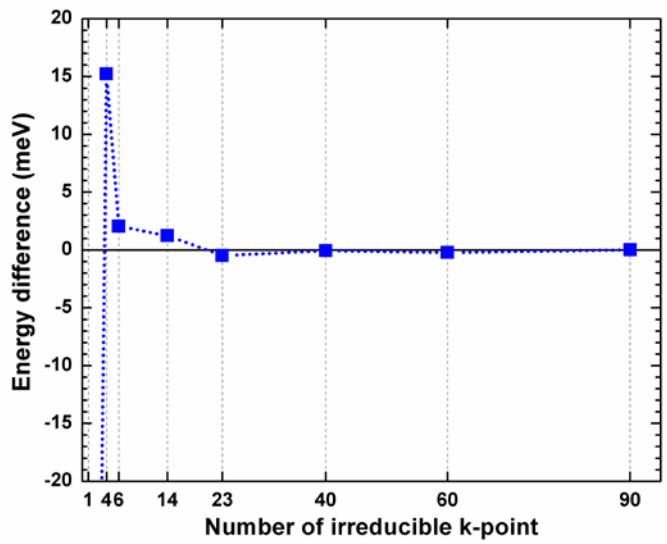

Figure 8. Difference in total energy obtained for CPO-27-Ni using different number of irreducible k-points: E(k=90) – E(k=i), with i = 1, 4, 6, 14, 23, 40, 60 and 90.

4.4. Multiplet ligand field calculations

Non resonant inelastic X-ray scattering (NIXS) spectra were calculated using the QUANTY code[44b, 85] while the RVtC-XES spectra were calculated using the XTLS code[86] in the framework of multiplet ligand-field theory using Wannier orbitals. In our calculations, we use material-specific model parameters obtained by means of a DFT and local cluster many-body model, including Ni(3*d*) orbitals with full on-site Coulomb interaction and metal local environment, treated as 10 composite ligand orbitals. The RVtC-XES spectra are calculated including the same orbitals as for NIXS calculation, considering also Ni(1*s*) states in order to allow intermediate states with core-hole in the Ni(1*s*) shell. The effect of the core hole on the *d-d* transitions is mainly in a rigid blue shift of the whole spectrum in the region from 0 to 6 eV due to the spherical shape of *s*-wave function. The structure of all compounds was optimized using DFT pseudopotential approach, implemented in VASP 5.3 code.[34a, 87] The spectra of CPO-27-Ni in interaction with adsorbed molecules have been obtained freezing the MOF framework structure to that optimized for the bare material. Adsorbed molecules were added at the geometry position obtained from DFT calculation. Small framework relaxation phenomena were consequently neglected. For all adsorbates, the distance Ni-adsorbate (R_{ads}) obtained with the VASP code (see Table 4) is similar to the value obtained by Valenzano et al.[17c] using CRYSTAL09 code.[33]

Table 4. Structural parameters for the models used in calculations. The Ni-O distances (only the average value $<R_O>_{VASP}$ is reported) were kept equal to those of the dehydrated form, while the position of the adsorbate molecules, distance Ni-adsorbate $(R_{ads})_{VASP}$, was fixed to the value obtained by the GGA-PBE VASP DFT geometry relaxation. For comparison, also EXAFS experimental data and theoretical structure optimization performed with CRYSTAL09 code are reported.

	NiO	Dehydrated	+H_2O	+CO	+NO	+H_2S
$<R_O>_{exp}$	–	2.00 [a]	2.03 [a]	2.024 [b]	2.00 [a]	–
$<R_O>_{VASP}$	2.08	2.00	2.00	2.00	2.00	2.00
$<R_O>_{CRYSTAL09}$		2.034 [c]	2.069 [c]	2.066 [c]	2.057 [c]	2.013 [d]
$(R_{ads})_{exp}$ [a]	–	–	2.10 [a]	2.11 [b]	1.87 [a]	2.590 [e]
$(R_{ads})_{VASP}$ [a]	–	–	2.15	2.15	2.11	2.54
$(R_{ads})_{CRYSTAL09}$ [a]	–	–	2.153 [c]	2.148 [c]	2.101 [c]	2.663 [d]

[a] Experimental values refer to the EXAFS results from Bonino et al.[16]
[b] Experimental values refer to the EXAFS results from Chavan et al.[17a]
[c] Theoretical periodic structure optimization perform with CRYSTAL09 code by Valenzano et al.[17c]
[d] Theoretical periodic structure optimization perform with CRYSTAL09 code by Chavan et al.[17d]
[e] Synchrotron powder XRD by Allan et al.[25]

These structures were used for band structure calculations by means of full potential linearized augmented plane wave (FLAPW) approach, implemented in Wien2k.[88] The set of Wannier orbitals has been constructed based on the delocalized Bloch functions using an algorithm for construction of maximally localized wavefunctions within the Wien2wannier interface[89] and the Wannier90 code.[90] Ni(*d*)- and O(*p*)-atomic orbitals were used as projectors for Wannier functions construction and the final result was verified by means of comparison between original band structure from FLAPW and that based on constructed Wannier functions. In order to construct the local basis of maximally localized Wannier functions, we take all bands within the energy window [–12.0 : +2.0] eV with respect to the Fermi level, forming the valence bands. Figure 9 shows an excellent agreement between these two approaches for the case of bare CPO-27.

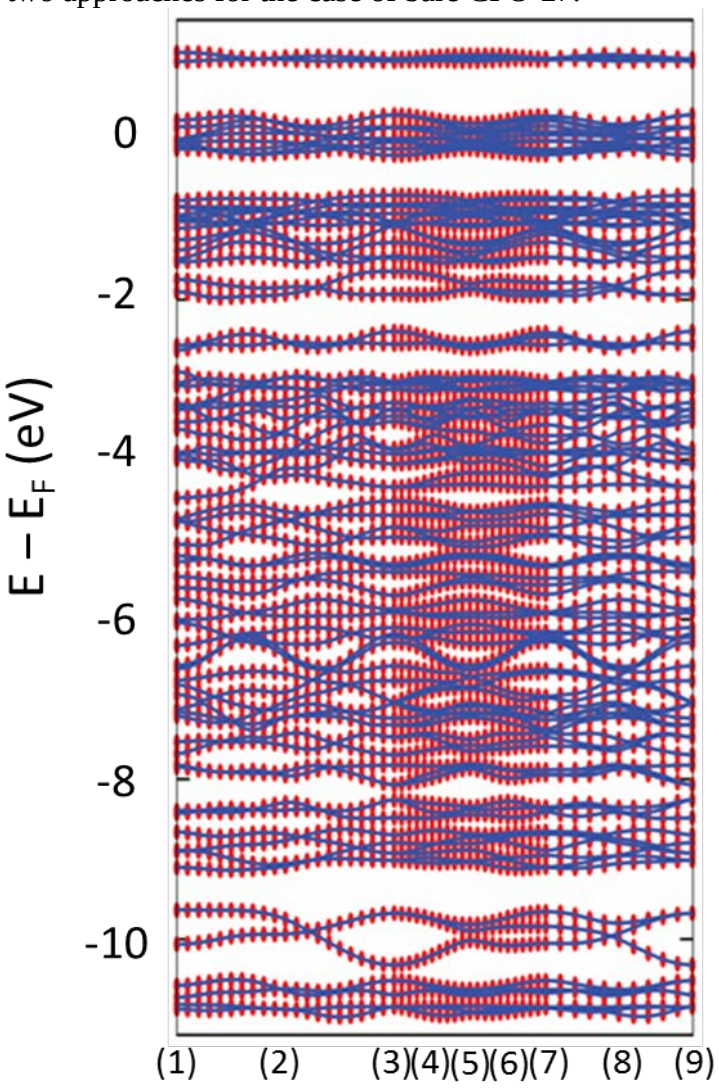

Figure 9. Comparison between the original band structure, obtained from WIEN2k (blue solid lines), and band structure based on Wannier functions (red dots). The abscissa axis corresponds to a pathway through nine symmetrical points: (1/2, 1/2, 1/2), (1/4, 1/4, 1/4), (0, 0, 0), (1/4, 0, 0), (1/2, 0, 0), (1/2, 1/4, 0), (1/2, 1/2, 0), (1/4, 1/4, 0), (0, 0, 0), identified as points (1)–(9) in the abscissa axis.

The models, based on Wannier functions described above, contain from 144 to 150 orbitals depending on the adsorbate. The corresponding structures, without rotational symmetries, contain up to 72 atoms. The models were then reduced to the minimal local models, containing five *d*-like orbitals of Ni and five molecular orbitals constructed from oxygen *p*-like states of the CPO-27 lattice nearest neighbors and molecular orbital of adsorbate (when present). Thus, for each structure, we obtain a 10×10 hopping matrix which is used subsequently in the multiplet calculations. Table 5

and Table 6 reports the 10×10 hopping matrix for the cases of perfect (in NiO) and distorted octahedron (hydrated CPO-27), respectively. The corresponding matrices for the bare CPO-27-Ni and CPO-27-Ni with CO, NO and H_2S adsorbates are reported in the SI. The grey part of the matrix represents five Ni(*d*)-like orbitals, the green part represents five ligand orbitals and the white parts are the hopping matrix elements between Ni(*d*)-like and ligand states.

Table 5. 10×10 hopping matrix based on minimal local model for NiO. This represent the case of a perfect octahedron. The grey part of the matrix represents five Ni(*d*)-like orbitals, the green part represents five ligand orbitals and the white parts are the hopping matrix elements between Ni(*d*)-like and ligand states.

-1.5	0.0	0.0	0.0	0.0	1.7	0.0	0.0	0.0	0.0
0.0	-1.5	0.0	0.0	0.0	0.0	1.7	0.0	0.0	0.0
0.0	0.0	-1.5	0.0	0.0	0.0	0.0	1.7	0.0	0.0
0.0	0.0	0.0	-1.0	0.0	0.0	0.0	0.0	2.9	0.0
0.0	0.0	0.0	0.0	-1.0	0.0	0.0	0.0	0.0	2.9
1.7	0.0	0.0	0.0	0.0	-4.3	0.4	0.4	0.0	0.0
0.0	1.7	0.0	0.0	0.0	0.4	-4.3	0.4	0.0	0.0
0.0	0.0	1.7	0.0	0.0	0.4	0.4	-4.3	0.0	0.0
0.0	0.0	0.0	2.9	0.0	0.0	0.0	0.0	-5.0	0.0
0.0	0.0	0.0	0.0	2.9	0.0	0.0	0.0	0.0	-5.0

Table 6. 10×10 hopping matrix based on minimal local model for hydrated CPO-27-Ni. This represent the case of a distorted octahedron. The grey part of the matrix represents five Ni(*d*)-like orbitals, the green part represents five ligand orbitals and the white parts are the hopping matrix elements between Ni(*d*)-like and ligand states.

-1.8	0.0	0.0	0.0	0.0	1.2	0.0	0.0	0.0	0.0
0.0	-1.6	0.0	0.0	0.0	0.0	1.1	0.0	0.1	0.0
0.0	0.0	-1.5	0.0	0.0	0.0	0.0	1.1	0.2	-0.1
0.0	0.0	0.0	-1.3	0.0	0.0	0.1	0.2	2.4	0.0
0.0	0.0	0.0	0.0	-1.0	0.0	0.0	-0.1	0.0	2.2
1.2	0.0	0.0	0.0	0.0	-6.3	0.2	0.0	0.0	0.3
0.0	1.1	0.0	0.1	0.0	0.2	-5.1	0.2	-0.3	-0.2
0.0	0.0	1.1	0.2	-0.1	0.0	0.2	-5.0	-0.3	0.0
0.0	0.1	0.2	2.4	0.0	0.0	-0.3	-0.3	-5.4	-0.1
0.0	0.0	-0.1	0.0	2.2	0.3	-0.2	0.0	-0.1	-6.5

Eq. (1) reports the local Hamiltonian of the system:

$$H = \sum_{i,j} \varepsilon_L(i,j) c_i^\dagger c_j + \sum_{i,j} \varepsilon_d(i,j) d_i^\dagger d_j + \sum_{i,j} V(i,j) c_i^\dagger d_j + \sum_{i,j,k,l} U(i,j,k,l) d_i^\dagger d_j d_k^\dagger d_l + \varepsilon_s s^\dagger s + \sum_{i,j} U_{sd}(i,j) s^\dagger s d_i^\dagger d_j + h.c. + \zeta \boldsymbol{L}_d \cdot \boldsymbol{S}_d \quad (1)$$

In Eq. (1), we consider a cluster model with a fixed number of 20 electrons. The local model accounts for: the hybridization between Ni(*d*) and ligand orbitals (first three terms); the full Coulomb $U_{d\text{-}d}$ interaction (fourth term); core-hole effects for XES (fifth and sixth terms); and the spin-orbit coupling at 3*d* shell (last term). U(i,j,k,l) is being parametrized via Slater integrals F(0),

F(2) and F(4).[91] The F(2) = 12.234 eV, F(4)=7.598 eV and ζ = 0.083 eV are taken from;[92] we used U_{3d3d}= 7.3 eV; consequently F(0) = U_{dd} + ($F2_{dd}$+$F4_{dd}$)·2/63.[93]

Resonant spectra are implemented by calculating a third order Green's function $G^3(\Omega,\omega)$, defined as:

$$G^3(\Omega,\omega) = \left\langle \psi_i \left| T_1^\dagger \frac{1}{\Omega - H_1 - i\Gamma/2} T_2^\dagger \frac{1}{\omega - H_2 + i\Gamma/2} T_2 \frac{1}{\Omega - H_1 + i\Gamma/2} T_1 \right| \psi_i \right\rangle \qquad (2)$$

where T_1 and T_2 are the transition operators from Ni(1*s*) to Ni(3*d*) and from Ni(3*d*) to Ni(1*s*), correspondingly (each transition operator is a product of a creation and annihilation operators), where Γ is an adjustable parameter for the lifetime broadening of the calculated spectra and where H_1 and H_2 are the Hamiltonians of the system in the ground state and intermediate state of the RVtC-RIXS process, see Figure 2c.

AUTHOR INFORMATION
Corresponding Authors
*E-mails: carlo.lamberti@unito.it
Notes
The authors declare no competing financial interest.

■ ACKNOWLEDGMENTS
This work was supported by FP7-NMP-2008-LARGE-2 collaborative project NanoMOF (Nanoporous Metal-Organic Frameworks for production) project number 228604. C.L., A.A.G. and A.L.B. acknowledge the Mega-grant of the Russian Federation Government to support scientific research at Southern Federal University, No. 14.Y26.31.0001. A.A.G. acknowledges the grant of the President of Russia for young scientists no. MK-7300.2016.2. We are indebted with Pieter Glatzel (ESRF) and with Silvia Bordiga (University of Turin) for in depth discussion on RVtC-XES and UV-Vis spectra respectively.

Table of Contents synopsis

For Table of Contents Only: The combination of UV-Vis and resonant valence to core X-ray emission spectroscopies, supported by theoretical calculations within ligand field multiplet theory, sheds light on the changes of the *d-d* transitions upon molecular adsorption on Ni^{2+} centers with a coordination vacancy hosted in MOFs.	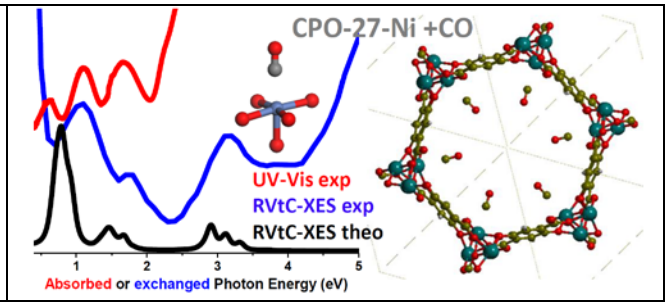

■ REFERENCES

(1) (a) Ferey, G., *Chem. Soc. Rev.* **2008,** *37*, 191-214; (b) Perry IV, J. J.; Perman, J. A.; Zaworotko, M. J., *Chem. Soc. Rev.* **2009,** *38*, 1400-1417; (c) Cavka, J. H.; Jakobsen, S.; Olsbye, U.; Guillou, N.; Lamberti, C.; Bordiga, S.; Lillerud, K. P., *J. Am. Chem. Soc.* **2008,** *130*, 13850-13851; (d) Murray, L. J.; Dinca, M.; Long, J. R., *Chem. Soc. Rev.* **2009,** *38*, 1294-1314; (e) Valenzano, L.; Civalleri, B.; Chavan, S.; Bordiga, S.; Nilsen, M. H.; Jakobsen, S.; Lillerud, K. P.; Lamberti, C., *Chem. Mat.* **2011,** *23*, 1700-1718; (f) O'Keeffe, M.; Yaghi, O. M., *Chem. Rev.* **2012,** *112*, 675-702; (g) Stock, N.; Biswas, S., *Chem. Rev.* **2012,** *112*, 933-969; (h) Cook, T. R.; Zheng, Y. R.; Stang, P. J., *Chem. Rev.* **2013,** *113*, 734-777; (i) Lu, W. G.; Wei, Z. W.; Gu, Z. Y.; Liu, T. F.; Park, J.; Park, J.; Tian, J.; Zhang, M. W.; Zhang, Q.; Gentle, T.; Bosch, M.; Zhou, H. C., *Chem. Soc. Rev.* **2014,** *43*, 5561-5593; (j) Butova, V. V.; Soldatov, M. A.; Guda, A. A.; Lomachenko, K. A.; Lamberti, C., *Russ. Chem. Rev.* **2016,** *85*, 280-307; (k) Schoedel, A.; Li, M.; Li, D.; O'Keeffe, M.; Yaghi, O. M., *Chem. Rev.* **2016**.
(2) Czaja, A.; Trukhan, T.; Müller, U., *Chem. Soc. Rev.* **2009,** *38*, 1284-1293.

(3) (a) Dietzel, P. D. C.; Johnsen, R. E.; Fjellvag, H.; Bordiga, S.; Groppo, E.; Chavan, S.; Blom, R., *Chem. Commun.* **2008**, 5125-5127; (b) Vitillo, J. G.; Regli, L.; Chavan, S.; Ricchiardi, G.; Spoto, G.; Dietzel, P. D. C.; Bordiga, S.; Zecchina, A., *J. Am. Chem. Soc.* **2008,** *130*, 8386-8396; (c) Nelson, A. P.; Farha, O. K.; Mulfort, K. L.; Hupp, J. T., *J. Am. Chem. Soc.* **2009,** *131*, 458-460; (d) Suh, M. P.; Park, H. J.; Prasad, T. K.; Lim, D. W., *Chem. Rev.* **2012,** *112*, 782-835; (e) Sumida, K.; Rogow, D. L.; Mason, J. A.; McDonald, T. M.; Bloch, E. D.; Herm, Z. R.; Bae, T. H.; Long, J. R., *Chem. Rev.* **2012,** *112*, 724-781; (f) Chavan, S.; Vitillo, J. G.; Gianolio, D.; Zavorotynska, O.; Civalleri, B.; Jakobsen, S.; Nilsen, M. H.; Valenzano, L.; Lamberti, C.; Lillerud, K. P.; Bordiga, S., *Phys. Chem. Chem. Phys.* **2012,** *14*, 1614-1626; (g) He, Y. B.; Zhou, W.; Qian, G. D.; Chen, B. L., *Chem. Soc. Rev.* **2014,** *43*, 5657-5678.
(4) (a) Dinca, M.; Long, J. R., *J. Am. Chem. Soc.* **2005,** *127*, 9376-9377; (b) Li, J. R.; Sculley, J.; Zhou, H. C., *Chem. Rev.* **2012,** *112*, 869-932.
(5) Kreno, L. E.; Leong, K.; Farha, O. K.; Allendorf, M.; Van Duyne, R. P.; Hupp, J. T., *Chem. Rev.* **2012,** *112*, 1105-1125.
(6) (a) Xiao, B.; Wheatley, P. S.; Zhao, X. B.; Fletcher, A. J.; Fox, S.; Rossi, A. G.; Megson, I. L.; Bordiga, S.; Regli, L.; Thomas, K. M.; Morris, R. E., *J. Am. Chem. Soc.* **2007,** *129*, 1203-1209; (b) Taylor-Pashow, K. M. L.; Della Rocca, J.; Xie, Z. G.; Tran, S.; Lin, W. B., *J. Am. Chem. Soc.* **2009,** *131*, 14261-14263; (c) Horcajada, P.; Chalati, T.; Serre, C.; Gillet, B.; Sebrie, C.; Baati, T.; Eubank, J. F.; Heurtaux, D.; Clayette, P.; Kreuz, C.; Chang, J. S.; Hwang, Y. K.; Marsaud, V.; Bories, P. N.; Cynober, L.; Gil, S.; Ferey, G.; Couvreur, P.; Gref, R., *Nat. Mater.* **2010,** *9*, 172-178; (d) Horcajada, P.; Gref, R.; Baati, T.; Allan, P. K.; Maurin, G.; Couvreur, P.; Ferey, G.; Morris, R. E.; Serre, C., *Chem. Rev.* **2012,** *112*, 1232-1268.
(7) (a) Bordiga, S.; Lamberti, C.; Ricchiardi, G.; Regli, L.; Bonino, F.; Damin, A.; Lillerud, K. P.; Bjorgen, M.; Zecchina, A., *Chem. Commun.* **2004**, 2300-2301; (b) Allendorf, M. D.; Bauer, C. A.; Bhakta, R. K.; Houk, R. J. T., *Chem. Soc. Rev.* **2009,** *38*, 1330-1352; (c) Cui, Y. J.; Yue, Y. F.; Qian, G. D.; Chen, B. L., *Chem. Rev.* **2012,** *112*, 1126-1162; (d) Hu, Z. C.; Deibert, B. J.; Li, J., *Chem. Soc. Rev.* **2014,** *43*, 5815-5840.
(8) (a) Kurmoo, M., *Chem. Soc. Rev.* **2009,** *38*, 1353-1379; (b) Coronado, E.; Espallargas, G. M., *Chem. Soc. Rev.* **2013,** *42*, 1525-1539.
(9) (a) Ferey, G.; Millange, F.; Morcrette, M.; Serre, C.; Doublet, M. L.; Greneche, J. M.; Tarascon, J. M., *Angew. Chem.-Int. Edit.* **2007,** *46*, 3259-3263; (b) Horike, S.; Umeyama, D.; Kitagawa, S., *Accounts Chem. Res.* **2013,** *46*, 2376-2384.
(10) (a) Horike, S.; Dinca, M.; Tamaki, K.; Long, J. R., *J. Am. Chem. Soc* **2008,** *130*, 5854-5855; (b) Lee, J.; Farha, O. K.; Roberts, J.; Scheidt, K. A.; Nguyen, S. T.; Hupp, J. T., *Chem. Soc. Rev.* **2009,** *38*, 1450-1459; (c) Ma, L.; Abney, C.; Lin, W., *Chem. Soc. Rev.* **2009,** *38*, 1248-1256; (d) Corma, A.; Garcıa, H.; Llabres i Xamena, F. X., *Chem. Rev.* **2010,** *110*, 4606-4655; (e) Yoon, M.; Srirambalaji, R.; Kim, K., *Chem. Rev.* **2012,** *112*, 1196-1231; (f) Llabrés i Xamena, F.; Gascon, J., *Metal Organic Frameworks as Heterogeneous Catalysts*. Royal Society of Chemistry: Cambridge, 2013; p 1-432; (g) Zhao, M.; Ou, S.; Wu, C. D., *Acc. Chem. Res.* **2014,** *47*, 1199-207; (h) Chughtai, A. H.; Ahmad, N.; Younus, H. A.; Laypkov, A.; Verpoort, F., *Chem. Soc. Rev.* **2015,** *44*, 6804-6849.
(11) (a) Sava, D. F.; Rodriguez, M. A.; Chapman, K. W.; Chupas, P. J.; Greathouse, J. A.; Crozier, P. S.; Nenoff, T. M., *J. Am. Chem. Soc.* **2011,** *133*, 12398-12401; (b) Jakobsen, J.; Gianolio, D.; Wragg, D.; Nilsen, M. H.; Emerich, H.; Bordiga, S.; Lamberti, C.; Olsbye, U.; Tilset, M.; Lillerud, K. P., *Phys. Rev. B* **2012,** *86*, art. n. 125429.
(12) (a) Kotani, A.; Shin, S., *Rev. Mod. Phys.* **2001,** *73*, 203-246; (b) Glatzel, P.; Bergmann, U., *Coord. Chem. Rev.* **2005,** *249*, 65-95; (c) Ament, L. J. P.; van Veenendaal, M.; Devereaux, T. P.; Hill, J. P.; van den Brink, J., *Rev. Mod. Phys.* **2011,** *83*, 705-767.
(13) (a) Dietzel, P. D. C.; Morita, Y.; Blom, R.; Fjellvag, H., *Angew. Chem.-Int. Edit.* **2005,** *44*, 6354-6358; (b) Dietzel, P. D. C.; Panella, B.; Hirscher, M.; Blom, R.; Fjellvag, H., *Chem. Commun.* **2006**, 959-961.
(14) (a) Rosi, N. L.; Kim, J.; Eddaoudi, M.; Chen, B. L.; O'Keeffe, M.; Yaghi, O. M., *J. Am. Chem. Soc.* **2005,** *127*, 1504-1518; (b) Dietzel, P. D. C.; Johnsen, R. E.; Blom, R.; Fjellvåg, H., *Chem. Eur. J.* **2008,** *14*, 2389-2397.
(15) (a) Valenzano, L.; Civalleri, B.; Chavan, S.; Palomino, G. T.; Arean, C. O.; Bordiga, S., *J. Phys. Chem. C* **2010,** *114*, 11185-11191; (b) Sanz, R.; Martínez, F.; Orcajo, G.; Wojtas, L.; Briones, D., *Dalton Trans.* **2013,** *42*, 2392-8; (c) Bloch, E. D.; Hudson, M. R.; Mason, J. A.; Chavan, S.; Crocella, V.; Howe, J. D.; Lee, K.; Dzubak, A. L.; Queen, W. L.; Zadrozny, J. M.; Geier, S. J.; Lin, L. C.; Gagliardi, L.; Smit, B.; Neaton, J. B.; Bordiga, S.; Brown, C. M.; Long, J. R., *J. Am. Chem. Soc.* **2014,** *136*, 10752-10761.
(16) Bonino, F.; Chavan, S.; Vitillo, J. G.; Groppo, E.; Agostini, G.; Lamberti, C.; Dietzel, P. D. C.; Prestipino, C.; Bordiga, S., *Chem. Mat.* **2008,** *20*, 4957-4968.
(17) (a) Chavan, S.; Vitillo, J. G.; Groppo, E.; Bonino, F.; Lamberti, C.; Dietzel, P. D. C.; Bordiga, S., *J. Phys. Chem. C* **2009,** *113*, 3292-3299; (b) Chavan, S.; Bonino, F.; Vitillo, J. G.; Groppo, E.; Lamberti, C.; Dietzel, P. D. C.; Zecchina, A.; Bordiga, S., *Phys. Chem. Chem. Phys.* **2009,** *11*, 9811-9822; (c) Valenzano, L.; Vitillo, J. G.; Chavan, S.; Civalleri, B.; Bonino, F.; Bordiga, S.; Lamberti, C., *Catal. Today* **2012,** *182*, 67-79; (d) Chavan, S.; Bonino, F.; Valenzano, L.; Civalleri, B.; Lamberti, C.; Acerbi, N.; Cavka, J. H.; Leistner, M.; Bordiga, S., *J. Phys. Chem. C* **2013,** *117*, 15615-15622.
(18) (a) Kapelewski, M. T.; Geier, S. J.; Hudson, M. R.; Stück, D.; Mason, J. A.; Nelson, J. N.; Xiao, D. J.; Hulvey, Z.; Gilmour, E.; FitzGerald, S. A.; Head-Gordon, M.; Brown, C. M.; Long, J. R., **2014,** *136*, 12119-29; (b) Lee, J. S.; Vlaisavljevich, B.; Britt, D. K.; Brown, C. M.; Haranczyk, M.; Neaton, J. B.; Smit, B.; Long, J. R.; Queen, W. L., *Adv. Mater.* **2015**.

(19) Bloch, E. D.; Queen, W. L.; Chavan, S.; Wheatley, P. S.; Zadrozny, J. M.; Morris, R.; Brown, C. M.; Lamberti, C.; Bordiga, S.; Long, J. R., *J. Am. Chem. Soc.* **2015,** *137*, 3466-3469.
(20) Bloch, E. D.; Murray, L. J.; Queen, W. L.; Chavan, S.; Maximoff, S. N.; Bigi, J. P.; Krishna, R.; Peterson, V. K.; Grandjean, F.; Long, G. J.; Smit, B.; Bordiga, S.; Brown, C. M.; Long, J. R., *J. Am. Chem. Soc.* **2011,** *133*, 14814-14822.
(21) (a) Zhou, W.; Wu, H.; Yildirim, T., *J. Am. Chem. Soc.* **2008,** *130*, 15268-15269; (b) Chavan, S. M.; Zavorotynska, O.; Lamberti, C.; Bordiga, S., *Dalton Trans.* **2013,** *42*, 12586-12595.
(22) (a) Dietzel, P. D. C.; Besikiotis, V.; Blom, R., *J. Mater. Chem.* **2009,** *19*, 7362-7370; (b) Britt, D.; Furukawa, H.; Wang, B.; Glover, T. G.; Yaghi, O. M., *Proc. Natl. Acad. Sci. U. S. A.* **2009,** *106*, 20637-20640; (c) Queen, W. L.; Hudson, M. R.; Bloch, E. D.; Mason, J. A.; Gonzalez, M. I.; Lee, J. S.; Gygi, D.; Howe, J. D.; Lee, K.; Darwish, T. A.; James, M.; Peterson, V. K.; Teat, S. J.; Smit, B.; Neaton, J. B.; Long, J. R.; Brown, C. M., *Chem. Sci.* **2014,** *5*, 4569-4581.
(23) Mangano, E.; Kahr, J.; Wright, P. A.; Brandani, S., *Faraday Discuss.* **2016,** *192*, 181-195.
(24) Chavan, S. M.; Shearer, G. C.; Bloch, E.; Bordiga, S., *ChemPhysChem* **2012,** *13*, 445-448.
(25) Allan, P. K.; Wheatley, P. S.; Aldous, D.; Mohideen, M. I.; Tang, C.; Hriljac, J. A.; Megson, I. L.; Chapman, K. W.; De Weireld, G.; Vaesen, S.; Morris, R. E., *Dalton Trans.* **2012,** *41*, 4060-4066.
(26) Van de Voorde, B.; Hezinová, M.; Lannoeye, J.; Vandekerkhove, A.; Marszalek, B.; Gil, B.; Beurroies, I.; Nachtigall, P.; De Vos, D., *Phys. Chem. Chem. Phys.* **2015,** *17*, 10759-66.
(27) (a) Rouquerol, F.; Rouquerol, J.; Sing, K., *Adsorption by Powders and Porous Solids Principles, Methodology and Applications*. Academic Press: London, 1999; (b) Bolis, V.; Barbaglia, A.; Bordiga, S.; Lamberti, C.; Zecchina, A., *J. Phys. Chem. B* **2004,** *108*, 9970-9983.
(28) (a) Garrone, E.; Otero Arean, C., *Chem. Soc. Rev.* **2005,** *34*, 846-857; (b) Bordiga, S.; Lamberti, C.; Bonino, F.; Travert, A.; Thibault-Starzyk, F., *Chem. Soc. Rev.* **2015,** *44*, 7262-7341.
(29) Ghose, S. K.; Li, Y.; Yakovenko, A.; Dooryhee, E.; Ehm, L.; Ecker, L. E.; Dippel, A. C.; Halder, G. J.; Strachan, D. M.; Thallapally, P. K., *J. Phys. Chem. Lett.* **2015,** *6*, 1790-4.
(30) (a) Rojas, S.; Wheatley, P. S.; Quartapelle-Procopio, E.; Gil, B.; Marszalek, B.; Morris, R. E.; Barea, E., *Crystengcomm* **2013,** *15*, 9364-9367; (b) Cattaneo, D.; Warrender, S. J.; Duncan, M. J.; Castledine, R.; Parkinson, N.; Haley, I.; Morris, R. E., *Dalton Trans.* **2016,** *45*, 618-629; (c) Cattaneo, D.; Warrender, S. J.; Duncan, M. J.; Kelsall, C. J.; Doherty, M. K.; Whitfield, P. D.; Megson, I. L.; Morris, R. E., *RSC Adv.* **2016,** *6*, 14059-14067.
(31) Elsayed, E.; Al-Dadah, R.; Mahmoud, S.; Anderson, P. A.; Elsayed, A.; Youssef, P. G., *Desalination* **2017,** *406*, 25-36.
(32) Xiao, D. J.; Bloch, E. D.; Mason, J. A.; Queen, W. L.; Hudson, M. R.; Planas, N.; Borycz, J.; Dzubak, A. L.; Verma, P.; Lee, K.; Bonino, F.; Crocellà, V.; Yano, J.; Bordiga, S.; Truhlar, D. G.; Gagliardi, L.; Brown, C. M.; Long, J. R., *Nat. Chem.* **2014,** *6*, 590-5.
(33) Dovesi, R.; Saunders, V. R.; Roetti, R.; Orlando, R.; Zicovich-Wilson, C. M.; Pascale, F.; Civalleri, B.; Doll, K.; Harrison, N. M.; Bush, I. J.; D'Arco, P.; Llunell, M., *CRYSTAL09, University of Torino, Torino* **2009**.
(34) (a) Kresse, G.; Furthmuller, J., *Phys. Rev. B* **1996,** *54*, 11169-11186; (b) Kresse, G.; Joubert, D., *Phys. Rev. B* **1999,** *59*, 1758-1775; (c) Hafner, J., *J. Comput. Chem.* **2008,** *29*, 2044-2078.
(35) Lee, K.; Murray, E. D.; Kong, L. Z.; Lundqvist, B. I.; Langreth, D. C., *Phys. Rev. B* **2010,** *82*, Art. n. 081101.
(36) Sumida, K.; Brown, C. M.; Herm, Z. R.; Chavan, S.; Bordiga, S.; Long, J. R., *Chem. Commun.* **2011,** *47*, 1157-1159.
(37) Arean, C. O.; Chavan, S.; Cabello, C. P.; Garrone, E.; Palomino, G. T., *ChemPhysChem* **2010,** *11*, 3237-3242.
(38) Peng, Y.; Krungleviciute, V.; Eryazici, I.; Hupp, J. T.; Farha, O. K.; Yildirim, T., *J. Am. Chem. Soc.* **2013,** *135*, 11887-94.
(39) Caskey, S. R.; Wong-Foy, A. G.; Matzger, A. J., *J. Am. Chem. Soc.* **2008,** *130*, 10870-10871.
(40) Valenzano, L.; Civalleri, B.; Sillar, K.; Sauer, J., *J. Phys. Chem. C* **2011,** *115*, 21777-21784.
(41) Simmons, J. M.; Wu, H.; Zhou, W.; Yildirim, T., *Energy Environ. Sci.* **2011,** *4*, 2177-2185.
(42) Mercado, R.; Vlaisayljevich, B.; Lin, L. C.; Lee, K.; Lee, Y.; Mason, J. A.; Xiao, D. J.; Gonzalez, M. I.; Kapelewski, M. T.; Neaton, J. B.; Smit, B., *J. Phys. Chem. C* **2016,** *120*, 12590-12604.
(43) Garino, C.; Borfecchia, E.; Gobetto, R.; van Bokhoven, J. A.; Lamberti, C., *Coord. Chem. Rev.* **2014,** *277*, 130-186.
(44) (a) de Groot, F., *Chem. Rev.* **2001,** *101*, 1779-1808; (b) Haverkort, M. W.; Zwierzycki, M.; Andersen, O. K., *Phys. Rev. B* **2012,** *85*, Art. n. 165113.
(45) Figgis, B. N., *Introduction to Ligand Fields*. Wiley-Interscience:: New York, 1967.
(46) (a) Groothaert, M. H.; van Bokhoven, J. A.; Battiston, A. A.; Weckhuysen, B. M.; Schoonheydt, R. A., *J. Am. Chem. Soc.* **2003,** *125*, 7629-7640; (b) Jentoft, F. C., *Adv. Catal.* **2009,** *52*, 129-211; (c) Schoonheydt, R. A., *Chem. Soc. Rev.* **2010,** *39*, 5051-5066.
(47) (a) Barone, V.; Polimeno, A., *Chem. Soc. Rev.* **2007,** *36*, 1724-1731; (b) Barone, V.; Improta, R.; Rega, N., *Accounts Chem. Res.* **2008,** *41*, 605-616.
(48) (a) Ricchiardi, G.; Damin, A.; Bordiga, S.; Lamberti, C.; Spanò, G.; Rivetti, F.; Zecchina, A., *J. Am. Chem. Soc.* **2001,** *123*, 11409-11419; (b) O'Shea, V. A. D.; Capel-Sanchez, M.; Blanco-Brieva, G.; Campos-Martin, J. M.; Fierro, J. L. G., *Angew. Chem.-Int. Edit.* **2003,** *42*, 5851-5854; (c) Salassa, L.; Garino, C.; Salassa, G.; Gobetto, R.;

Nervi, C., *J. Am. Chem. Soc.* **2008,** *130*, 9590-9597; (d) Chavan, S.; Vitillo, J. G.; Uddin, M. J.; Bonino, F.; Lamberti, C.; Groppo, E.; Lillerud, K. P.; Bordiga, S., *Chem. Mat.* **2010,** *22*, 4602-4611.
(49) Leofanti, G.; Padovan, M.; Garilli, M.; Carmello, D.; Zecchina, A.; Spoto, G.; Bordiga, S.; Palomino, G. T.; Lamberti, C., *J. Catal.* **2000,** *189*, 91-104.
(50) Escalona Platero, E.; Spoto, G.; Coluccia, S.; Zecchina, A., *Langmuir* **1987,** *3*, 291-291.
(51) Ghiringhelli, G.; Matsubara, M.; Dallera, C.; Fracassi, F.; Gusmeroli, R.; Piazzalunga, A.; Tagliaferri, A.; Brookes, N. B.; Kotani, A.; Braicovich, L., *J. Phys.: Condens. Matter* **2005,** *17*, 5397.
(52) Huotari, S.; Pylkkanen, T.; Vanko, G.; Verbeni, R.; Glatzel, P.; Monaco, G., *Phys. Rev. B* **2008,** *78*, Art. No. 041102.
(53) Mino, L.; Agostini, G.; Borfecchia, E.; Gianolio, D.; Piovano, A.; Gallo, E.; Lamberti, C., *J. Phys. D-Appl. Phys.* **2013,** *46*, 423001.
(54) van Veenendaal, M.; Liu, X. S.; Carpenter, M. H.; Cramer, S. P., *Phys. Rev. B* **2011,** *83*, Art. No. 045101.
(55) (a) Duda, L. C.; Schmitt, T.; Magnuson, M.; Forsberg, J.; Olsson, A.; Nordgren, J.; Okada, K.; Kotani, A., *Phys. Rev. Lett.* **2006,** *96*, Art. No. 067402; (b) Lundberg, M.; Kroll, T.; DeBeer, S.; Bergmann, U.; Wilson, S. A.; Glatzel, P.; Nordlund, D.; Hedman, B.; Hodgson, K. O.; Solomon, E. I., *J. Am. Chem. Soc.* **2013,** *135*, 17121-17134; (c) Glatzel, P.; Weng, T. C.; Kvashnina, K.; Swarbrick, J.; Sikora, M.; Gallo, E.; Smolentsev, N.; Mori, R. A., *J. Electron Spectrosc. Relat. Phenom.* **2013,** *188*, 17-25; (d) Gallo, E.; Bonino, F.; Swarbrick, J. C.; Petrenko, T.; Piovano, A.; Bordiga, S.; Gianolio, D.; Groppo, E.; Neese, F.; Lamberti, C.; Glatzel, P., *ChemPhysChem* **2013,** *14*, 79-83; (e) Lomachenko, K. A.; Garino, C.; Gallo, E.; Gianolio, D.; Gobetto, R.; Glatzel, P.; Smolentsev, N.; Smolentsev, G.; Soldatov, A. V.; Lamberti, C.; Salassa, L., *Phys. Chem. Chem. Phys.* **2013,** *15*, 16152-16159; (f) Gallo, E.; Glatzel, P., *Adv. Mater.* **2014,** *26*, 7730-7746; (g) Bordiga, S.; Groppo, E.; Agostini, G.; van Bokhoven, J. A.; Lamberti, C., *Chem. Rev.* **2013,** *113*, 1736-1850.
(56) (a) Heijboer, W. M.; Glatzel, P.; Sawant, K. R.; Lobo, R. F.; Bergmann, U.; Barrea, R. A.; Koningsberger, D. C.; Weckhuysen, B. M.; de Groot, F. M. F., *J. Phys. Chem. B* **2004,** *108*, 10002-10011; (b) Heijboer, W. M.; Koningsberger, D. C.; Weckhuysen, B. M.; de Groot, F. M. F., *Catal. Today* **2005,** *110*, 228-238; (c) Pirngruber, G. D.; Grunwaldt, J. D.; van Bokhoven, J. A.; Kalytta, A.; Reller, A.; Safonova, O. V.; Glatzel, P., *J. Phys. Chem. B* **2006,** *110*, 18104-18107; (d) Pirngruber, G. D.; Grunwaldt, J. D.; Roy, P. K.; van Bokhoven, J. A.; Safonova, O.; Glatzel, P., *Catal. Today* **2007,** *126*, 127-134; (e) Glatzel, P.; Sikora, M.; Smolentsev, G.; Fernandez-Garcia, M., *Catal. Today* **2009,** *145*, 294-299; (f) Glatzel, P.; Singh, J.; Kvashnina, K. O.; van Bokhoven, J. A., *J. Am. Chem. Soc.* **2010,** *132*, 2555-2557; (g) Gallo, E.; Lamberti, C.; Glatzel, P., *Phys. Chem. Chem. Phys.* **2011,** *13*, 19409-19419; (h) Seenivasan, K.; Gallo, E.; Piovano, A.; Vitillo, J. G.; Sommazzi, A.; Bordiga, S.; Lamberti, C.; Glatzel, P.; Groppo, E., *Dalton Trans.* **2013,** *42*, 12706-12713; (i) Gallo, E.; Piovano, A.; Marini, C.; Mathon, O.; Pascarelli, S.; Glatzel, P.; Lamberti, C.; Berlier, G., *J. Phys. Chem. C* **2014,** *118*, 11745-11751; (j) Frenkel, A. I.; van Bokhoven, J. A., *J. Synchrot. Radiat.* **2014,** *21*, 1084-1089; (k) Small, M. W.; Kas, J. J.; Kvashnina, K. O.; Rehr, J. J.; Nuzzo, R. G.; Tromp, M.; Frenkel, A. I., *ChemPhysChem* **2014,** *15*, 1569-1572; (l) Groppo, E.; Seenivasan, K.; Gallo, E.; Sommazzi, A.; Lamberti, C.; Bordiga, S., *ACS Catal.* **2015,** *5*, 5586-5595; (m) Groppo, E.; Gallo, E.; Seenivasan, K.; Lomachenko, K. A.; Sommazzi, A.; Bordiga, S.; Glatzel, P.; van Silfhout, R.; Kachatkou, A.; Bras, W.; Lamberti, C., *ChemCatChem* **2015,** *7*, 1432-1437; (n) Borfecchia, E.; Lomachenko, K. A.; Giordanino, F.; Falsig, H.; Beato, P.; Soldatov, A. V.; Bordiga, S.; Lamberti, C., *Chem. Sci.* **2015,** *6*, 548-563; (o) Giordanino, F.; Borfecchia, E.; Lomachenko, K. A.; Lazzarini, A.; Agostini, G.; Gallo, E.; Soldatov, A. V.; Beato, P.; Bordiga, S.; Lamberti, C., *J. Phys. Chem. Lett.* **2014,** *5*, 1552-1559; (p) Janssens, T. V. W.; Falsig, H.; Lundegaard, L. F.; Vennestrom, P. N. R.; Rasmussen, S. B.; Moses, P. G.; Giordanino, F.; Borfecchia, E.; Lomachenko, K. A.; Lamberti, C.; Bordiga, S.; Godiksen, A.; Mossin, S.; Beato, P., *ACS Catal.* **2015,** *5*, 2832-2845; (q) Lomachenko, K. A.; Borfecchia, E.; Negri, C.; Berlier, G.; Lamberti, C.; Beato, P.; Falsig, H.; Bordiga, S., *J. Am. Chem. Soc.* **2016,** *138*, 12025-12028; (r) Lomachenko, K. A.; Borfecchia, E.; Bordiga, S.; Soldatov, A. V.; Beato, P.; Lamberti, C., *J. Phys.:Conf. Ser.* **2016,** *712*, 012041.
(57) Swarbrick, J. C.; Kvashnin, Y.; Schulte, K.; Seenivasan, K.; Lamberti, C.; Glatzel, P., *Inorg. Chem.* **2010,** *49*, 8323-8332.
(58) (a) Zhang, G. P.; Callcott, T. A.; Woods, G. T.; Lini, L.; Sales, B.; Mandrus, D.; He, J., *Phys. Rev. Lett.* **2002,** *88*, 077401; (b) Augustsson, A.; Henningsson, A.; Butorin, S. M.; Siegbahn, H.; Nordgren, J.; Guo, J. H., *J. Chem. Phys.* **2003,** *119*, 3983-3987; (c) Kuepper, K.; Falub, M. C.; Prince, K. C.; Galakhov, V. R.; Troyanchuk, I. O.; Chiuzbaian, S. G.; Matteucci, M.; Wett, D.; Szargan, R.; Ovechkina, N. A.; Mukovskii, Y. M.; Neumann, M., *J. Phys. Chem. B* **2005,** *109*, 9354-9361; (d) Ghiringhelli, G.; Matsubara, M.; Dallera, C.; Fracassi, F.; Tagliaferri, A.; Brookes, N. B.; Kotani, A.; Braicovich, L., *Phys. Rev. B* **2006,** *73*, 035111; (e) Chiuzbaian, S. G.; Schmitt, T.; Matsubara, M.; Kotani, A.; Ghiringhelli, G.; Dallera, C.; Tagliaferri, A.; Braicovich, L.; Scagnoli, V.; Brookes, N. B.; Staub, U.; Patthey, L., *Phys. Rev. B* **2008,** *78*, 245102; (f) Hague, C. F.; Mariot, J. M.; Ilakovac, V.; Delaunay, R.; Marsi, M.; Sacchi, M.; Rueff, J. P.; Felsch, W., *Phys. Rev. B* **2008,** *77*, 045132; (g) Thakur, P.; Bisogni, V.; Cezar, J. C.; Brookes, N. B.; Ghiringhelli, G.; Gautam, S.; Chae, K. H.; Subramanian, M.; Jayavel, R.; Asokan, K., *J. Appl. Phys.* **2010,** *107*, 103915; (h) Gretarsson, H.; Clancy, J. P.; Liu, X.; Hill, J. P.; Bozin, E.; Singh, Y.; Manni, S.; Gegenwart, P.; Kim, J.; Said, A. H.; Casa, D.; Gog, T.; Upton, M. H.; Kim, H. S.; Yu, J.; Katukuri, V. M.; Hozoi, L.; van den Brink, J.; Kim, Y. J., *Phys. Rev. Lett.* **2013,** *110*, 076402; (i) Li, J.; Sham, T. K.; Ye, Y. F.; Zhu, J. F.; Guo, J. H., *J. Phys. Chem. C* **2015,** *119*, 2222-2230.

(59) (a) Grenier, S.; Hill, J. P.; Kiryukhin, V.; Ku, W.; Kim, Y. J.; Thomas, K. J.; Cheong, S. W.; Tokura, Y.; Tomioka, Y.; Casa, D.; Gog, T., *Phys. Rev. Lett.* **2005,** *94*, 047203; (b) Hancock, J. N.; Chabot-Couture, G.; Li, Y.; Petrakovskii, G. A.; Ishii, K.; Jarrige, I.; Mizuki, J.; Devereaux, T. P.; Greven, M., *Phys. Rev. B* **2009,** *80*, 092509; (c) Chabot-Couture, G.; Hancock, J. N.; Mang, P. K.; Casa, D. M.; Gog, T.; Greven, M., *Phys. Rev. B* **2010,** *82*, 035113; (d) Chen, C. C.; Moritz, B.; Vernay, F.; Hancock, J. N.; Johnston, S.; Jia, C. J.; Chabot-Couture, G.; Greven, M.; Elfimov, I.; Sawatzky, G. A.; Devereaux, T. P., *Phys. Rev. Lett.* **2010,** *105*, 177401; (e) Kim, J. H.; Ellis, D. S.; Gog, T.; Casa, D.; Kim, Y. J., *Phys. Rev. B* **2010,** *81*, 073109; (f) Mino, L.; Colombo, V.; Vitillo, J. G.; Lamberti, C.; Bordiga, S.; Gallo, E.; Glatzel, P.; Maspero, A.; Galli, S., *Dalton Trans.* **2012,** *41*, 4012-4019.

(60) (a) Kuiper, P.; Guo, J. H.; Sathe, C.; Duda, L. C.; Nordgren, J.; Pothuizen, J. J. M.; de Groot, F. M. F.; Sawatzky, G. A., *Phys. Rev. Lett.* **1998,** *80*, 5204-5207; (b) Wang, H. X.; Young, A. T.; Guo, J. H.; Cramer, S. P.; Friedrich, S.; Braun, A.; Gu, W. W., *J. Synchrot. Radiat.* **2013,** *20*, 614-619.

(61) Gallo, E.; Lamberti, C.; Glatzel, P., *Inorg. Chem.* **2013,** *52*, 5633-5635.

(62) Oien, S.; Agostini, G.; Svelle, S.; Borfecchia, E.; Lomachenko, K. A.; Mino, L.; Gallo, E.; Bordiga, S.; Olsbye, U.; Lillerud, K. P.; Lamberti, C., *Chem. Mat.* **2015,** *27*, 1042-1056.

(63) (a) Shadle, S. E.; Hedman, B.; Hodgson, K. O.; Solomon, E. I., *J. Am. Chem. Soc.* **1995,** *117*, 2259-2272; (b) Gorelsky, S. I.; Basumallick, L.; Vura-Weis, J.; Sarangi, R.; Hodgson, K. O.; Hedman, B.; Fujisawa, K.; Solomon, E. I., *Inorg. Chem.* **2005,** *44*, 4947-4960; (c) van Bokhoven, J. A.; Lamberti, C., *Coord. Chem. Rev.* **2014,** *277*, 275-290.

(64) (a) Bordiga, S.; Coluccia, S.; Lamberti, C.; Marchese, L.; Zecchina, A.; Boscherini, F.; Buffa, F.; Genoni, F.; Leofanti, G.; Petrini, G.; Vlaic, G., *J. Phys. Chem.* **1994,** *98*, 4125-4132; (b) Bordiga, S.; Damin, A.; Bonino, F.; Zecchina, A.; Spanò, G.; Rivetti, F.; Bolis, V.; Lamberti, C., *J. Phys. Chem. B* **2002,** *106*, 9892-9905; (c) George, S. D.; Brant, P.; Solomon, E. I., *J. Am. Chem. Soc.* **2005,** *127*, 667-674; (d) George, S. D.; Huang, K. W.; Waymouth, R. M.; Solomon, E. I., *Inorg. Chem.* **2006,** *45*, 4468-4477; (e) Bordiga, S.; Bonino, F.; Damin, A.; Lamberti, C., *Phys. Chem. Chem. Phys.* **2007,** *9*, 4854-4878.

(65) (a) Laubach, S.; Schmidt, P. C.; Thissen, A.; Fernandez-Madrigal, F. J.; Wu, Q. H.; Jaegermann, W.; Klemm, M.; Horn, S., *Phys. Chem. Chem. Phys.* **2007,** *9*, 2564-2576; (b) Murayama, H.; Vitry, D.; Ueda, W.; Fuchs, G.; Anne, M.; Dubois, J. L., *Appl. Catal. A-Gen.* **2007,** *318*, 137-142; (c) Si, C.; Xu, W.; Wang, H.; Zhou, J.; Ablat, A.; Zhang, L. J.; Cheng, J.; Pan, Z. Y.; Fan, L. L.; Zou, C. W.; Wu, Z. Y., *Phys. Chem. Chem. Phys.* **2012,** *14*, 15021-15028.

(66) (a) Peterson, M. L.; Brown, G. E.; Parks, G. A.; Stein, C. L., *Geochim. Cosmochim. Acta* **1997,** *61*, 3399-3412; (b) Pantelouris, A.; Modrow, H.; Pantelouris, M.; Hormes, J.; Reinen, D., *Chem. Phys.* **2004,** *300*, 13-22; (c) Groppo, E.; Lamberti, C.; Bordiga, S.; Spoto, G.; Zecchina, A., *Chem. Rev.* **2005,** *105*, 115-183; (d) Groppo, E.; Prestipino, C.; Cesano, F.; Bonino, F.; Bordiga, S.; Lamberti, C.; Thune, P. C.; Niemantsverdriet, J. W.; Zecchina, A., *J. Catal.* **2005,** *230*, 98-108; (e) Agostini, G.; Groppo, E.; Bordiga, S.; Zecchina, A.; Prestipino, C.; D'Acapito, F.; van Kimmenade, E.; Thune, P. C.; Niemantsverdriet, J. W.; Lamberti, C., *J. Phys. Chem. C* **2007,** *111*, 16437-16444; (f) Gianolio, D.; Groppo, E.; Vitillo, J. G.; Damin, A.; Bordiga, S.; Zecchina, A.; Lamberti, C., *Chem. Commun.* **2010,** *46*, 976-978.

(67) (a) Gilbert, B.; Frazer, B. H.; Belz, A.; Conrad, P. G.; Nealson, K. H.; Haskel, D.; Lang, J. C.; Srajer, G.; De Stasio, G., *J. Phys. Chem. A* **2003,** *107*, 2839-2847; (b) Glatzel, P.; Bergmann, U.; Yano, J.; Visser, H.; Robblee, J. H.; Gu, W. W.; de Groot, F. M. F.; Christou, G.; Pecoraro, V. L.; Cramer, S. P.; Yachandra, V. K., *J. Am. Chem. Soc.* **2004,** *126*, 9946-9959; (c) Yano, J.; Robblee, J.; Pushkar, Y.; Marcus, M. A.; Bendix, J.; Workman, J. M.; Collins, T. J.; Solomon, E. I.; George, S. D.; Yachandra, V. K., *J. Am. Chem. Soc.* **2007,** *129*, 12989-13000.

(68) (a) Bordiga, S.; Buzzoni, R.; Geobaldo, F.; Lamberti, C.; Giamello, E.; Zecchina, A.; Leofanti, G.; Petrini, G.; Tozzola, G.; Vlaic, G., *J. Catal.* **1996,** *158*, 486-501; (b) Westre, T. E.; Kennepohl, P.; DeWitt, J. G.; Hedman, B.; Hodgson, K. O.; Solomon, E. I., *J. Am. Chem. Soc.* **1997,** *119*, 6297-6314.

(69) (a) Le Toquin, R.; Paulus, W.; Cousson, A.; Prestipino, C.; Lamberti, C., *J. Am. Chem. Soc.* **2006,** *128*, 13161-13174; (b) Sarangi, R.; Cho, J.; Nam, W.; Solomon, E. I., *Inorg. Chem.* **2011,** *50*, 614-620.

(70) (a) Colpas, G. J.; Maroney, M. J.; Bagyinka, C.; Kumar, M.; Willis, W. S.; Suib, S. L.; Baidya, N.; Mascharak, P. K., *Inorg. Chem.* **1991,** *30*, 920-928; (b) Gu, Z. J.; Dong, J.; Allan, C. B.; Choudhury, S. B.; Franco, R.; Moura, J. J. G.; LeGall, J.; Przybyla, A. E.; Roseboom, W.; Albracht, S. P. J.; Axley, M. J.; Scott, R. A.; Maroney, M. J., *J. Am. Chem. Soc.* **1996,** *118*, 11155-11165; (c) Sanchez, M. C.; Garcia, J.; Blasco, J.; Subias, G.; Perez-Cacho, J., *Phys. Rev. B* **2002,** *65*, 9.

(71) (a) Lamberti, C.; Spoto, G.; Scarano, D.; Paze, C.; Salvalaggio, M.; Bordiga, S.; Zecchina, A.; Palomino, G. T.; DAcapito, F., *Chem. Phys. Lett.* **1997,** *269*, 500-508; (b) Turnes Palomino, G.; Fisicaro, P.; Bordiga, S.; Zecchina, A.; Giamello, E.; Lamberti, C., *J. Phys. Chem. B* **2000,** *104*, 4064-4073; (c) Prestipino, C.; Berlier, G.; Llabrés i Xamena, F. X.; Spoto, G.; Bordiga, S.; Zecchina, A.; Palomino, G. T.; Yamamoto, T.; Lamberti, C., *Chem. Phys. Lett.* **2002,** *363*, 389-396; (d) Llabrés i Xamena, F. X.; Fisicaro, P.; Berlier, G.; Zecchina, A.; Palomino, G. T.; Prestipino, C.; Bordiga, S.; Giamello, E.; Lamberti, C., *J. Phys. Chem. B* **2003,** *107*, 7036-7044.

(72) Gougoussis, C.; Calandra, M.; Seitsonen, A.; Brouder, C.; Shukla, A.; Mauri, F., *Phys. Rev. B* **2009,** *79*, Art. No. 045118.

(73) Bonino, F.; Damin, A.; Ricchiardi, G.; Ricci M; Spanò G; D'Aloisio R; Zecchina A; Lamberti C; Prestipino C; Bordiga, S., *J. Phys. Chem. B* **2004,** *108*, 3573-3583.

(74) Ciampolini, M., *Inorg. Chem.* **1966,** *5*, 35-40.

(75) Bordiga, S.; Bonino, F.; Lillerud, K. P.; Lamberti, C., *Chem. Soc. Rev.* **2010,** *39*, 4885-4927.

(76) Guda, S. A.; Guda, A. A.; Soldatov, M. A.; Lomachenko, K. A.; Bugaev, A. L.; Lamberti, C.; Gawelda, W.; Bressler, C.; Smolentsev, G.; Soldatov, A. V.; Joly, Y., *J. Chem. Theory Comput.* **2015,** *11*, 4512-4521.
(77) Bonino, F.; Lamberti, C.; Chavan, S.; Vitillo, J. G.; Bordiga, S., Characterization of MOFs. 1. Combined Vibrational and Electronic Spectroscopies. In *Metal Organic Frameworks as Heterogeneous Catalysts*, Llabrés i Xamena, F.; Gascon, J., Eds. Royal Soc Chemistry: Cambridge, 2013; pp 76-142.
(78) Groppo, E.; Gallo, E.; Seenivasan, K.; Lomachenko, K. A.; Sommazzi, A.; Bordiga, S.; Glatzel, P.; van Silfhout, R.; Kachatkou, A.; Bras, W.; Lamberti, C., *ChemCatChem* **2015,** *7*, 1432-1437.
(79) Filipponi, A.; Borowski, M.; Bowron, D. T.; Ansell, S.; Di Cicco, A.; De Panfilis, S.; Itie, J. P., *Rev. Sci. Instrum.* **2000,** *71*, 2422-2432.
(80) Lamberti, C.; Prestipino, C.; Bordiga, S.; Berlier, G.; Spoto, G.; Zecchina, A.; Laloni, A.; La Manna, F.; D'Anca, F.; Felici, R.; D'Acapito, F.; Roy, P., *Nucl. Instrum. Methods B* **2003,** *200*, 196-201.
(81) Perdew, J. P.; Burke, K.; Ernzerhof, M., *Phys. Rev. Lett.* **1996,** *77*, 3865-3868.
(82) Dudarev, S. L.; Botton, G. A.; Savrasov, S. Y.; Humphreys, C. J.; Sutton, A. P., *Phys. Rev. B* **1998,** *57*, 1505-1509.
(83) Anisimov, V. I.; Gunnarsson, O., *Phys. Rev. B* **1991,** *43*, 7570-7574.
(84) Grimme, S.; Antony, J.; Ehrlich, S.; Krieg, H., *J. Chem. Phys.* **2010,** *132*, Art. n. 154104.
(85) (a) Haverkort, M. W.; Sangiovanni, G.; Hansmann, P.; Toschi, A.; Lu, Y.; Macke, S., *Europhys. Lett.* **2014,** *108*, Art. n. 57004; (b) Lu, Y.; Hoppner, M.; Gunnarsson, O.; Haverkort, M. W., *Phys. Rev. B* **2014,** *90*, Art. n. 085102.
(86) (a) Tanaka, A.; Jo, T., *J. Phys. Soc. Jpn.* **1994,** *63*, 2788-2807; (b) Kobayashi, M.; Niwa, H.; Takeda, Y.; Fujimori, A.; Senba, Y.; Ohashi, H.; Tanaka, A.; Ohya, S.; Hai, P. N.; Tanaka, M.; Harada, Y.; Oshima, M., *Phys. Rev. Lett.* **2014,** *112*, Art. n. 107203.
(87) Kresse, G.; Furthmuller, J., *Comput. Mater. Sci.* **1996,** *6*, 15-50.
(88) (a) Schwarz, K.; Blaha, P.; Madsen, G. K. H., *Comput. Phys. Commun.* **2002,** *147*, 71-76; (b) Schwarz, K.; Blaha, P., *Comput. Mater. Sci.* **2003,** *28*, 259-273; (c) Schwarz, K., *J. Solid State Chem.* **2003,** *176*, 319-328.
(89) Kunes, J.; Arita, R.; Wissgott, P.; Toschi, A.; Ikeda, H.; Held, K., *Comput. Phys. Commun.* **2010,** *181*, 1888-1895.
(90) (a) Mostofi, A. A.; Yates, J. R.; Lee, Y. S.; Souza, I.; Vanderbilt, D.; Marzari, N., *Comput. Phys. Commun.* **2008,** *178*, 685-699; (b) Mostofi, A. A.; Yates, J. R.; Pizzi, G.; Lee, Y. S.; Souza, I.; Vanderbilt, D.; Marzari, N., *Comput. Phys. Commun.* **2014,** *185*, 2309-2310.
(91) (a) Cowan, R. D., *J. Opt. Soc. Am.* **1968,** *58*, 808-818; (b) Cowan, R. D., *The Theory of Atomic Structure and Spectra*. University of California Press: Berkeley, 1981.
(92) Haverkort, M. W.; Tanaka, A.; Tjeng, L. H.; Sawatzky, G. A., *Phys. Rev. Lett.* **2007,** *99*, Art. n. 257401.
(93) (a) Mizokawa, T., *Ph .D. thesis, Groningen* **1985**; (b) van der Marel, D., *Ph .D. thesis, Groningen* **1985**.